INDEPENDENT COMPONENT ANALYSIS (ICA) IN ANALYSING CHILD HIGH-DENSITY EVENT-RELATED POTENTIAL (ERP) AND CURRENT SOURCE DENSITY (CSD) DATA

Annika Tanskanen
Master's thesis
Department of Psychology
University of Jyväskylä
Spring 2008

Supervisor of the graduate thesis	Paavo H.T. Leppänen, Docent, Ph.D., Academy Research Fellow, Department of Psychology, University of Jyväskylä, Finland
Research project	3rd grade ERP-studies, Jyväskylä Longitudinal Study of Dyslexia (JLD) funded by Academy of Finland
Research site	Centre of Excellence for Human Development and Risk Factors, Department of Psychology, University of Jyväskylä, Finland

CONTENTS:

ABSTRACT 4

1. INTRODUCTION 5

1.1. Event-related potential (ERP) components 5
1.2. Current source density (CSD) analysis of ERPs 9
1.3. Methods for identifying and separating ERP components 11
1.4. Independent component analysis (ICA) 12
1.5. Aims of the study 16

2. METHODS 16

2.1. Participants 16
2.2. Experiment and stimuli 17
2.3. EEG recording and preprocessing 18
2.4. Data analysis 19

3. RESULTS 21

3.1. Visual inspection of grand averaged ERP waveforms and topographies 22
3.2. Visual inspection of grand averaged CSD waveforms and topographies 23
3.3. Identification of ERP-ICA and CSD-ICA N1 sub-components 26

4. DISCUSSION 42

REFERENCES 52

ABSTRACT

Author: Annika Tanskanen
Master's Thesis in Psychology
University of Jyväskylä
Spring 2008
57 pages

This Master's thesis focuses on studying independent component analysis (ICA) in analysing high-density averaged auditory event-related potential (ERP) and current source density (CSD) data. The applicability of ICA was studied in a theory driven and descriptive manner in attempt to isolate auditory N1 sub-components into independent components. The data analysed in this study was collected from 20 healthy 9-year-old children participating in the Jyväskylä Longitudinal Study of Dyslexia. The analysis were focused to responses to the first syllable /a/ of the /atta/-stimulus that was presented with equal probability with a long ISI varying pseudo-randomly between 1 and 5 seconds and as a standard in an oddball paradigm with a short ISI of 610 ms. ICA was applied separately to averaged ERP waveforms and their CSD transformations, in order to investigate which of the approaches, ERP-ICA or CSD-ICA, would lead to a better decomposition of the N1 sub-components into biologically plausible independent components. ICA components representing N1 activation were identified by visual inspection of their topographical scalp maps and temporal activation patterns, and grouped together to form clusters consisting of similar components reflecting the same underlying process in different participants. The selection of the N1-ICA components was guided by prior knowledge in the literature of the activation of the N1 sub-components in children. Both ERP-ICA and CSD-ICA solutions produced interpretable ICA components that were associated to activation of underlying brain structures related to N1 sub-components. ERP-ICA and CSD-ICA N1-clusters both included components activating at temporal, supratemporal and frontal areas. In addition, clusters with parietal and vertex components were decomposed only with ERP-ICA approach. Overall, the CSD-ICA approach summarised the N1 activation into more defined and localised ICA components when compared to the broadly distributed topographies of the ERP-ICA components. Results of this Master's thesis suggest that it is informative to contrast both ERP and CSD data in clarifying the nature of ERP generators.

Keywords: independent component analysis (ICA), developmental auditory event-related potentials (ERPs), current source density (CSD), auditory N1, N1b, non-specific N1, T-complex, children

---

1. INTRODUCTION

1.1. Event-related potential (ERP) components

Measuring brain waves, called event-related potentials (ERPs), is a means of getting information about brain's electrical activity in time with a precision of tens of milliseconds (Regan, 1989). The ERPs are brain responses temporally associated to stimulus events presented to a participant. They can be extracted from electroencephalogram (EEG) by averaging. When averaging EEG epochs related to a certain stimulus event, random electrical activity will approach zero, leaving the enhanced time-locked ERP signal visible. The ERP waveforms consist of a series of positive and negative voltage deflections that differ in amplitude, latency, and scalp distribution. The ERP deflections are a sum of electrical activity that reflects the activation of brain generators elicited by the stimulus.

The ERPs are traditionally classified into *exogenous* and *endogenous components* (Coles, Gratton, & Fabiani, 1990). Exogenous components are relatively stable obligatory components that are automatically elicited by the physical properties of a stimulus without attention being paid to the stimulus. Endogenous components, on the other hand, reflect cognitive processing and they can be elicited also in the absence of an external stimulus. The ERP components are typically named after their polarity (P for positivity; N for negativity) and latency or ordinal number of their occurrence in time.

The ERP component structure in children differs from that of adults. In the course of maturation, exogenous components go through developmental changes and new components appear. As described by Cheour, Leppänen, & Kraus (2000) and Ponton, Eggermont, Khosla, Kwong, & Don (2002) the latencies and amplitudes of the ERP components change during the development. The latencies of ERP components shorten with maturation, which is suggested to be due to increasing myelinisation and synaptic density with age. Age-related changes in the amplitudes of the ERP components on the other hand follow an inverted U-shape with the amplitude first increasing to reach its maxima prior to maturity and then decreasing again.

In the following sections, a brief description of some well-known ERP components is provided. The main emphasis is on a negative component called N1, which is in the focus of

this master's thesis and thus described more profoundly. After the introduction to ERP components, main attention is turned to methods that are used for extracting the ERP components from EEG.

The earliest components in the auditory ERP are exogenous brainstem responses that reflect the arrival of sensory input to cochlea and brainstem. They are followed by mid latency responses that are supposedly generated by the medial geniculate nucleus and the primary auditory cortex (Näätänen, 1990). The first long-latency exogenous peak in ERP is called *P1*, which is suggested to reflect auditory pre-perceptual sensory processing (Čeponienė, Rinne, & Näätänen, 2002). The P1 is generated by a tangential source located in the secondary auditory cortex in the lateral portion of Heschl's gyrus (Liegeois-Chauvel, Musolino, Badier, Marquis, & Chauvel, 1994; Ponton et al., 2002) and it can be recorded from central and frontal scalp sites. In children the P1 is recorded at the latency of 80 ms (Ponton et al., 2002).

The P1 is followed by a negative ERP deflection called *N1*, which is elicited about 100 ms after the stimulus onset in adults. Several studies indicate that the latency of N1 decreases as a function of age (Bruneau & Gomot, 1998; Čeponienė et al., 2002; Johnstone, Barry, Anderson, & Coyle, 1996; Ponton, Eggermont, Kwong, & Don, 2000; Sharma, Kraus, McGee, & Nicol, 1997). The N1 is an obligatory component and it is presumed to be linked with general conscious auditory sound level change detection and orienting of attention (Näätänen & Picton, 1987). The N1 can be elicited by a change in sound or silence; i.e. by an onset of a stimulus or a change in continuous sound, and also by an offset of a stimulus. The auditory N1 is sensitive to stimulus intensity and rate of stimulus presentation (Näätänen & Picton, 1987). Several studies indicate that there are more than one generator contributing to the scalp-recorded auditory N1 (Eggermont & Ponton, 2002; McCallum & Curry, 1980; Näätänen & Picton, 1987; Wolpaw & Penry, 1975). Supratemporal, vertex, lateral temporal and frontal sub-components have been identified.

Supratemporal component of N1 is called *N1b* and it is generated by bilateral tangentially oriented dipoles located in the supratemporal plane of the auditory cortex (Hari, Kaila, Katila, Tuomisto, & Varpula, 1982; Näätänen & Picton, 1987; Scherg & von Cramon, 1985; Vaughan & Ritter, 1970). It is suggested that also frontal generators may contribute to N1b (Bender, Oelkers-Ax, Resch, & Weisbrod, 2006). In ERP, the supratemporal N1b is generally observed as a negativity at frontocentral site reversing in polarity over the Sylvian fissure and being positive at temporomastoid areas (Bruneau & Gomot, 1998; Näätänen & Picton, 1987).

In a few studies, however, the N1b negativity in children have been seen at parietal areas instead (Daruna & Rau, 1987; Goodin, Squires, Henderson, & Starr 1978; Hämäläinen, Leppänen, Guttorm, & Lyytinen, 2007; Pang & Taylor, 2000). In current source density (CSD) maps, the N1b is seen as a current sink and source at temporoparietal areas also reversing in polarity over the Sylvian fissure (Giard et al., 1994). (For a description of the scalp current density method, see the next section.) According to Ponton et al. (2002), the N1b in children matures slowly. It is suggested by Bruneau and Gomot (1998), that in order for N1b to be elicited in children, the stimuli need to be presented with an interstimulus interval (ISI) over 1 second. With fast stimulation rate, the N1b first becomes identifiable at the age of 9 years as a small inflection of the positive P1 wave (Ponton et al., 2002). According to Bruneau and Gomot (1998), the N1b in 9-year-old children peaks at the latency of 110 ms. The supratemporal N1b component is thought to be associated with stimulus-specific sensory memory formation (Näätänen & Picton, 1987) or pre-attentive sound detection (Näätänen, 1990).

With long ISIs, the predominance of the N1 shifts posteriorly and the frontocentral component is overlapped by a modality *non-specific* N1 component. In ERP, the non-specific N1 is elicited as a widespread negativity at the vertex. Karhu et al. (1997) studied N1 vertex response to intermittent trains of four identical tone pips presented with ISI of 1 s and intertrain interval of 12 s. In 9-year-old children, a prominent N1 that was elicited at 130 ms at the vertex by the first tone of the train decreased by roughly 50 % in amplitude after the second tone, demonstrating the long refractory period of the non-specific component. In consequence of shortening the ISI, the latency of N1 was also slightly shortened (Karhu et al., 1997). According to Näätänen and Picton (1987), the non-specific N1 is most profoundly elicited with ISIs exceeding 4 ms. The generator of the non-specific N1 component is unknown, but a radial source perpendicular to the vertex is suggested by Hari et al. (1982). Involvement of motor and premotor cortices (Näätänen & Picton, 1987) and pre-frontal lobe (Alcaini, Giard, Thévenet, & Pernier, 1994) have also been suggested. The non-specific N1 component is thought be related to arousal mechanisms (Näätänen & Picton, 1987) and orienting of attention (Näätänen, 1990).

Temporal component of the N1 is called *T-complex*. The T-complex is generated radially in the superior temporal gyrus in the auditory association cortex of the lateral part of the temporal lobe (Wolpaw & Penry, 1975). It comprises of a series of negative and positive peaks (N1a, Ta and N1c) peaking at anterior temporal regions (Tonnquist-Uhlen, Ponton,

Eggermont, Kwong, & Don, 2003). Bruneau and Gomot (1998) and Pang and Taylor (2000) have studied T-complex maturation in children. In 7-9-year-old children, the T-complex peaks during a latency range of 75-170 ms (Bruneau & Gomot, 1998). In the study of Bruneau and Gomot (1998), the N1a of 7-9-year-old children was elicited at 75 ms with ISI varying between 1-2 seconds. The distribution of the N1a was dominated by activity at the left hemisphere. Using shorter ISI of 600 ms, Pang and Taylor (2002) reported that N1a negativity in 9-10-year old children was seen around the latency of 100 ms at both hemispheres. The positivity seen at temporal areas after N1a is called Ta. It peaks at the time window of the N1b. However, the Ta is produced by a radial source, which is separate from the tangential temporal positivity associated with N1b (Ponton et al., 2002). In children, the Ta is dominated by right hemisphere activity (Bruneau & Gomot, 1998). A second negative temporal peak is referred as N1c. In 7-10-year-old children it peaks at both hemispheres at the latency of 170 ms (Bruneau & Gomot, 1998; Pang and Taylor, 2000). In the study of Karhu et al. (1997), the N1c, recorded from 9-year-old children with an electrode at the left temporal hemisphere, was larger to the first tone of the train (inter-train-interval of 12 s) decreasing with tone repetition (ISI of 1 s). The temporal component of N1 can be recorded from children even with short ISI (Pang et al., 2000; Ponton et al., 2002; Tonnquist-Uhlen et al., 2003). In the literature, it has been suggested that the T-complex might be merely an inversion of vertex P1-N1b-P2 components but its independence is also supported (Ponton et al., 2002; Tonnquist-Uhlen et al., 2003).

Evidence of frontal lobe involvement during auditory N1 time window derives from current source density studies of Alcaini et al. (1994) and Bender et al. (2006) and Giard et al. (1994), all using 1000 Hz tone bursts as stimuli with varying ISIs. Alcaini et al. (1994) reported activation of two different frontal components in adults elicited with ISIs varying between 1 s up to 2 min in separate runs. First frontal component with mid frontal distribution was elicited for all ISIs at 95 ms while the other frontal component with more central distribution peaking at 140 ms was elicited only by stimuli presented with ISIs over 4 s. In the study of Giard et al. (1994), frontal contribution to N1 was studied in adults using ISI of 1 s eliciting only one frontal component, which peaked bilaterally during the time window of 65-125 ms. Bender et al., (2006) studied maturation of N1 frontal components in children using ISI varying between 10 to 15 s. Their study indicates that the first frontal component of N1 activating around N1b time window at mid-frontocentral site is nearly absent in children under 12 years whereas the second frontal component with mid-frontal sink peaking 40 - 50 ms after N1b is already well developed in 6-year-old children. Bender et al. (2006) suggested that the first frontal

component could be part of the frontocentral N1b component. The second frontal component contributing to N1 is suggested to be part of the non-specific N1 component with possible generators in anterior cinculate (Alcaini et al., 1994; Bender et al., 2006).

N1 is followed by *P2*, a second positive component in ERP, activating at central and frontal scalp sites. In 9-year-old children the P2 can be recorded at 180 ms (Hämäläinen et al., 2007). The P2 is generated in the Heschl's gyrus in the secondary auditory cortex in the temporal lobe (Lutkenhöner & Steinsträter, 1998) and it is produced by a tangential dipole (Ponton, et al., 2002). The most predominant peak in the ERP of children is the *N2*. It is a second negative peak of ERP peaking in children at the latency of 250 ms (Čeponienė et al., 2002). The N2 is not significantly attenuated with a fast stimulus rate like the N1 (Picton, Hillyard, Krausz, & Galambos, 1974). Karhu et al. (1997) have demonstrated that the N2 of 9-year-old children in fact increases in size, sensitizates, as a function of stimulus repetition. Like the N1, the N2 also has a frontocentral distribution (Čeponienė, Alku, Westerfield, Torki, & Townsend, 2005) and bilateral sources in the supratemporal auditory cortex (Bruneau & Gomot, 1998) that are produced by a tangential dipole (Ponton, et al., 2002). The N2 is thought to reflect sound content feature processing and synthesizing of sound features into a representation (Čeponienė et al., 2005).

As already mentioned, the activations of ERP components overlap with each other in time and space summing up to produce the observable ERP waveform. Also by the time the signals from different component generators reach the recording electrodes at the scalp, they have become even more fused together via volume conduction. The volume conduction is due to different conductivity in cortex, dura material, skull and scalp which blurs the signals and distributes them more widely over the scalp (Nunez & Srinivasan, 2006). The overlap of the ERP components and the volume conduction of their signals make it difficult to study a single component without first separating it from the rest of the ERP. In the following sections, first a description of a means for deblurring ERP topographies is provided and finally methods for identification and separation of the components from the ERP are introduced.

1.2. Current source density (CSD) analysis of ERPs

Despite the use of high-density EEG recordings, spatial resolution of ERP topography is nevertheless low due to volume conduction. Scalp potentials may also get distorted due to a

choice of a recording reference acting as a spatial filter and filtering out spatial components of the potential distributed over the scalp (Nunez & Srinivasan, 2006). To enhance spatial resolution of the ERP and overcome the problem of choosing the right reference, a reference-free spatial deblurring technique called current source density estimation (also known as scalp current density estimation) has been introduced. Current source density (CSD) transformation technique is based on algorithms that are derived from a negative second spatial (Laplacian) derivative of interpolated scalp potentials (Perrin, Pernier, Bertrand, & Echallier, 1989). The CSD waveforms are estimates of the current injected radially into the scalp from the underlying neuronal generators (Perrin et al., 1989). Sources and sinks in the CSD topography represent magnitude of radial current flow entering (sink) and leaving (source) the scalp (Nunez, 1981). Units of the current source density are voltage per unit distance (e.g. $\mu V/cm^2$). According to Nunez and Srinivasan (2006), the CSD waveforms are a good estimate of the durapotential i.e. the potential as it would be measured from the surface below the skull without being distorted by the volume conduction in the skull and the scalp. The estimated CSD waveforms are useful in sharpening and summarising the broad ERP voltage topographies. However, acting as a spatial filter, CSD emphasises EEG signals that are generated by superficial sources of the brain projecting to relatively small areas of cortex, while activity of sources deep in the brain or produced by broad dipole layers may not be captured (Srinivasan, 2005).

CSD transformation has previously been used successfully in analyzing auditory ERP data. Law, Rohrbaugh, Adams, & Eckardt (1993) showed that CSD transformation improves both spatial and temporal resolution of evoked EEG responses and also provide a better estimate of underlying cortical activity than potential waveforms. Kayser and Tenke (2006) compared principal component analysis (PCA) performed to ERP averages and their CSD transformations in order to evaluate the effectiveness of these solutions in separating ERP generator patterns. (For a description of the use of principal component analysis, see the following section.) Kayser and Tenke (2006) found that both ERP-PCA and CSD-PCA solutions resulted in very similar and equally interpretable factors. However, the CSD-PCA factors showed less temporal overlap and sharper and simpler topographies without losing or distorting any effects of interest. This lead Kayser and Tenke (2006) to conclude that CSD transformation proved to be a valuable preprocessing step for PCA.

1.3. Methods for identifying and separating ERP components

Next, an overview of methods for identification and separation of underlying components from ERP are provided. Classical peak amplitude and latency measurements and difference wave calculation are conventional methods used in ERP analysis that typically focus on a small number of channels. Principal component analysis (PCA) and independent component analysis (ICA), on the other hand, are methods that are more sophisticated and better suited in analysing high-density ERP data.

Classical peak measurement technique defines components mainly in terms of peak-amplitude and peak-latency measures of observable ERP deflections (Coles et al., 1990). This approach has proven to be problematic though, because as is known, the observable ERP deflections sum up the activity from several overlapping ERP components. Thus an amplitude at a latency at which the voltage reaches its maximum cannot be considered as a good reflection of time course and magnitude of a single underlying ERP component (Luck, 2005b), not even when CSD transformations of ERPs are used. This problem of component overlap can be overcome in certain cases by using difference waves in component identification. For example, a component that is known to occur in one experimental condition, but not in the other, can be isolated by subtracting the ERP waveforms obtained in these different conditions (Coles et al., 1990). However, when analysing peak and difference wave measures, the statistical analysis are applied only to a small number of channels in selected time windows which does not make good use of high-density ERP recordings.

To get more profound information about ERP components, one can apply the more advanced component identification methods based on functional relationships such as principal component analysis (PCA). PCA exploits the correlational structure of ERP or CSD waveforms to identify common patterns of covariance across participants, conditions and scalp locations (Coles et al., 1990). PCA takes into account all information in the dataset and distributes it ideally into a set of maximally decorrelating factors (i.e. PCA components) that presumably reflect the underlying ERP components. The PCA factors are derived by grouping together amplitude values at ERP time points (temporal PCA) or at electrodes (spatial PCA) that tend to vary in a correlated manner, as would be expected from the time points or scalp locations reflecting a common cognitive process. PCA allocates the greatest variance of the data to the first factor, the greatest variance of the remaining data variance to the second factor and so on, until the whole variance of the ERP dataset is explained. After the initial

actor extraction the solution must be rotated in order to maximise the chance that each factor reflects a single underlying component (Dien & Frishkoff, 2005). For a more detailed description of the application of PCA to ERP data, see Donchin and Heffley (1978). However, there are some limitations in PCA. Particularly problematic is, that PCA, instead of a single unique set of components, produces several solutions depending on which rotation is applied. Thus, additional assumptions are needed to decide on a particular rotation over another and according to Luck (2005a), there is typically no way to verify that the assumptions are correct.

During the last decade, a relatively new method called independent component analysis (ICA) has emerged in the analysis of ERP data. ICA too is based on the functional relationships like PCA, and it has, in fact, sometimes been referred to as an advanced and more sophisticated extension of PCA. In comparison to PCA, which is based on linear relations, ICA uses both linear and non-linear relations in the identification of components. While PCA removes only second-order correlations, ICA also minimizes higher order dependencies resulting in components that are not only decorrelating but also statistically maximally independent of each other (Makeig, Jung, Bell, Ghahremani, & Sejnowski, 1997). The percentage of the data variance each independent component accounts for, is much more homogenous in ICA than in PCA. In addition, ICA components are uniquely defined and thus do not need factor rotation (Stone, 2002). In the next section, a more detailed description of ICA methodology is provided.

1.4. Independent component analysis (ICA)

Independent component analysis (ICA) is a method of blind source separation that separates linearly mixed sources into maximally independent components. ICA can be used to analyse both raw EGG and averaged ERP data. When applied to raw EEG data, ICA is useful in identifying artefacts and isolating components that are not time-locked to the stimulus. Averaging, on the other hand, filters out non-time-locked activity, allowing ICA to focus on separating time-locked neural components. Applying ICA to averaged ERP data is useful in studying intersubject variability, whereas applying ICA to raw EEG data provides information on intertrial variability (Johnson et al., 2001). ICA tells of which spatially fixed and temporally independent activations the recorded EEG/ERP is composed of, but it does not tell where in the brain these activations arise.

ICA assumptions. There are four main assumptions underlying application of ICA (Brown, Yamada, & Sejnowski, 2001; Makeig et al., 1999; Jung et al., 2001). 1) Signals must be mixed linearly and instantaneously at the sensors. 2) Source activations must be spatially stationary and temporally independent. 3) Distributions of the source activations must be non-Gaussian. 4) Number of the sources must be equal to or less than the number of the recorded mixtures. For ERP analysis, the first ICA assumption is met by volume conduction which causes the signals to spread widely over the scalp. The volume conduction assures that summation of the signals at scalp sensors is linear, and that signal conduction times are equal, leaving no time delays between sources and mixing process at sensors. The second ICA assumption of the spatially stationary sources is compatible with the general assumption of ERP generators being spatially fixed. The temporal independence of the sources assumed by ICA, on the other hand, may be hard to fully achieve in case of averaged ERP data where the ERP components may have overlapping active periods. However, the temporal independence can be sufficiently enhanced by systematically varying the experimental stimuli and conditions thus minimizing the temporal overlap of the resulting averaged ERP components. In addition, worth noting is that, the data to be decomposed has to contain enough data points for the temporal independence of the ERP components to be expressed (for criteria, see below). According to the third ICA assumption, source distributions of recorded signals must be non-Gaussian, i.e. super- or sub-Gaussian, because ICA cannot separate multiple Gaussian processes (Hyvärinen & Oja, 2000). This is based on the Central Limit Theorem argument which states that any mixture of two independent distributions should produce a distribution that is closer to Gaussian than either of the original distributions alone. Therefore, distributions that are furthest from the Gaussian are most likely to be as statistically independent as possible (Jung et al., 2001). Averaged ERPs are generally assumed to be composed of one or more overlapping series of relatively brief activations which have a super-Gaussian distribution, but they can also include sub-Gaussian components like line noise, sensor noise and low frequency activity (Jung et al., 1998). Finally, according to the fourth ICA assumption, the number of recording sensors must be at least equal to the number of sources in the data. If there are less sensors than there are sources, the data becomes over-complete and ICA fails to decompose the sources into independent components.

ICA model. An introduction to a general ICA model can be found in the reviews of Brown et al. (2001), Onton, Westerfield, Townsend, & Makeig (2006) and Stone (2002). The task of the independent component analysis is to recover independent source signals **s** after they are

linearly mixed by an unknown matrix **A,** by only knowing the recorded signals **x**, **x=As**. Nothing is known about the sources or the mixing processes, except that there are *N* different recorded mixtures. When analysing EEG, this means recovering scalp distribution of underlying brain sources after the source signals are linearly mixed on the scalp by volume conduction. Scalp recorded EEG forms the ICA input data matrix **x** where the rows are signals recorded at different electrodes and columns are the signals recorded at different time points. The task of ICA is to find an unmixing matrix **W**, which linearly inverts the original source mixing process into the independent components **u**, **u=Wx**. In the search of this unmixing matrix, ICA uses only spatial information and several algorithms actually shuffle the time points before proceeding to the analysis.

A guideline to how much data is needed for successful ICA decomposition can be found in Onton et al. (2006). When data from *N* electrodes is decomposed, the number of time points in the input data has to be sufficiently large in order for ICA to be able to learn the N^2 weights of the unmixing matrix **W**. Onton et al. (2006) have suggested that the number of time points needed to decompose data from a large number of electrodes should be at least $20 \times N^2$. In case there is not enough data available for a complete ICA decomposition, one can pre-process the data using principal component analysis (PCA) to reduce the dimensionality of the data into a smaller number of its largest principal components.

Extended infomax algorithm. There are several different algorithms for ICA decomposition (Lee, Girolami, Bell, & Sejnowski, 2000; Onton et al., 2006). The ICA algorithm used in this study is a simple neural network learning algorithm called Extended infomax algorithm which blindly separates the measured signals into independent components using information maximization. The goal of this algorithm is to maximize the mutual information that the outputs of the neural network processor (measured signals **x**) contain about their inputs (underlying brain sources **s**). The mutual information between the inputs **s** and the outputs **x** of the neural processor can be maximised by maximizing the joint entropy of the outputs alone, $H(\mathbf{x})$, which in turn minimizes the mutual information among the ICA output components (Bell & Sejnowski, 1995; Lee et al., 2000). When mutual information between the ICA output components is zero, the components are considered to be statistically independent (Hyvärinen & Oja, 2000). ICA algorithms separate independent components from a set of mixed signals by finding a square unmixing matrix **W** that inverts the source mixing process (Onton et al., 2006). Extended infomax ICA algorithm is based on a general learning rule proposed by Bell and Sejnowski (1995) which is extended with applying the

natural gradient by Amari (1998) and the stability analysis by Cardoso and Laheld (1996) which allows switching between sub- and super-Gaussian distributions (Lee, Girolami, & Sejnowski, 1999). Extended infomax algorithm uses small randomly drawn batches of the recorded data to train the algorithm and adjust the unmixing matrix **W** in a stepwise learning manner until the entropy of the measured signals is maximized. At the end of the training, ICA multiplies the input data matrix **x** with the unmixing matrix **W**, linearly unmixing the recorded EEG into a sum of temporally and spatially fixed components, $\mathbf{u} = \mathbf{Wx}$ (Onton et al., 2006).

Outputs of the ICA model. The outputs of the ICA model are described e.g. in the reviews of Brown et al. (2001) and Onton et al. (2006). Rows of the ICA output data matrix **u** are called component activations and they give a spatially constant temporal activation pattern of the ICA components. These ICA component activations are similar to the factor weights produced by spatial principal component analysis (PCA). The inverse ICA unmixing matrix $\mathbf{W}^{-1}$ corresponds to the original source mixing matrix, $\mathbf{A} = \mathbf{W}^{-1}$, up to a permutation and a scale change. Columns of the unmixing matrix $\mathbf{W}^{-1}$ give a temporally constant projection strengths of the respective components onto the scalp sensors. The projection strengths of the components are arbitrary since ICA does not preserve scale. The projection of *i*th independent component onto the original data channels in the original recorded units (e.g. μV) can be attained by multiplying the *i*th row of the component activation matrix **u** with the *i*th column of the inverse unmixing matrix $\mathbf{W}^{-1}$. The sum of all projected components reconstructs the original data.

When applying ICA to ERP data, ICA is known to be prone to point out intersubject variability due to an inevitable differences between participants in recorded EEG signals. An electrode placed on the very same scalp location in every participant is likely to pick up different mixtures and strengths of equivalent EEG sources as a result of a unique folding of every brain and differences in orientation of functionally analogous sources within participants. Thus the strengths of different ICA component scalp maps and activation time courses are explicitly variable across participants and different participants contribute to different ICA components (Onton et al., 2006).

Limitations of ICA. Like any correlation-based method, ICA too encounters some limitations. For example, when two or more sources contribute to ERP averages at the same latency, ICA may capture them into a single component even if they occur in different locations of the

brain and represent different functions (Delorme & Makeig, 2004; Luck, 2005a). Furthermore, according to Luck (2005a), if a single component varies in latency across conditions, it may be treated by ICA as multiple components. Nevertheless, ICA is shown to be an effective tool for independent component decomposition of ERP data.

1.5. Aims of the study

This study was conducted to investigate the use of independent component analysis (ICA) method in the analysis of high-density averaged child auditory ERP data. The applicability of ICA was studied in a theory driven descriptive manner in attempt to isolate the auditory N1 sub-components. ICA was applied to two different types of input data, ERP waveforms and their CSD transformations. The aim was to investigate which of the approaches, ERP-ICA or CSD-ICA, would better decompose the auditory N1 component into biologically plausible independent components.

Knowing that some auditory N1 sub-components in children are sensitive to changes in ISI, different experimental conditions were used in order to tease out the N1 sub-components. It was hypothesised that a supratemporal N1b at 110 ms, a non-specific vertex-response at 130 ms and a radial temporal T-complex at the latency range of 80 - 170 ms would be elicited with long ISI, while only a radial temporal T-complex and maybe a small supratemporal N1b would be observed in short ISI condition at the same latencies than in the long ISI condition (Bruneau & Gomot, 1998; Karhu et al., 1997; Näätänen & Picton, 1987; Pang et al., 2000; Ponton et al., 2002; Tonnquist-Uhlen, et al, 2003). ICA was hypothesised to extract N1-ICA components at least from the large N1 elicited in the long ISI condition. It was assumed that ICA performed to CSD transformations would produce more precise and sharply defined components, since CSD maps by themselves are more precise and sharper in topography than broad ERP voltage maps.

2. METHODS

2.1. Participants

The ERP data analysed in this study was collected from 20 healthy 9-year-old children at 3rd grade participating in the ERP studies of Jyväskylä Longitudinal Study of Dyslexia (JLD) research project (Hämäläinen et al., 2007; Hämäläinen, Leppänen, Guttorm, & Lyytinen., 2008; Leinonen et al., 2001; Lyytinen et al., 2004). Approximately 200 children participating in the JLD-project were selected to the study even before their birth and followed up until adolescence. Half of these children had a familial risk for dyslexia, while the other half were born to families with similar backgrounds but with no incidents of dyslexia (Leinonen et al., 2001). Participants in this Master's thesis were 20 healthy children (9 boys, 11 girls) with a mean age of 9,4 years (range: 9,1 – 9,8 years) that had no familial risk for dyslexia, no reported neurological problems, and no reading or speech perception deficits.

2.2. Experiment and stimuli

Experiment. The ERP experiment consisted of five consecutive conditions: two speech conditions, two non-speech conditions and an equal probability condition (Hämäläinen et al., 2007; Hämäläinen et al., 2008). The interest of this study is limited only to the speech stimuli presented in speech and equal probability conditions which are described in more detail below. Duration of the experiment was approximately three hours in total including net application. During the experiment, participants watched a self-selected silent video or played a silent computer game. They were instructed not to pay any attention to the sounds. The stimuli were presented with the intensity of 75 dBA via a loud speaker located about 80 - 90 centimetres above the participant's head.

Stimuli. The speech stimuli used were naturally produced pseudowords /ata/, /apa/, /atta/ and /appa/. The pseudowords /ata/ and /apa/ were 300 ms in duration consisting of a first part of 72 ms including an initial glottal stop and a vowel /a/, a voiceless stop with a silent period of 95 ms and a second part of 133 ms including an explosion of /t/ in /ata/ or the explosion of /p/ in /apa/ and a final vowel /a/. The /atta/ and /appa/ stimuli were 460 ms in duration and they were artificially produced from /ata/ and /apa/ by lengthening the silent gap from 95 ms to

255 ms. Other acoustical aspects such as fundamental frequency and intensity were held constant (for further details, see Leppänen et al., 2002).

Experimental conditions. In the two speech conditions, stimuli were presented in an oddball paradigm in 5 blocks consisting of a total of 1000 standard stimuli and 250 deviant stimuli of two types, 125 stimuli per each deviant. The offset-to-onset interstimulus interval (ISI) was 610 ms. In the */ata/-condition* the standard stimulus was /ata/ occurring with an 80 % probability and the deviant stimuli were pseudo-randomly occurring /atta/ and /apa/ both occurring with a 10 % probability. In the */atta/-condition* the standard stimulus was /atta/ and the deviant stimuli were /ata/ and /appa/ (the probabilities of occurrence same as above). In the *equal probability (EQ) -condition* the stimuli from the */ata/-* and */atta/-conditions* (plus from the two non-speech conditions not analysed in this study) were presented with an equal probability paradigm with a probability of occurrence 12,5 %. Each stimulus was presented 80 times with ISI varying pseudo-randomly between 1 and 5 seconds.

2.3. EEG recording and preprocessing

EEG recording. The EEG data was collected with an Electric Geodesics Inc. (EGI) EEG-system (http://www.egi.com/) using Ag-AgCl electrodes attached to the EGI 128-channel sensor net. The data was recorded with NetStation 2.0 software (http://www.egi.com/netstation.html/). The sampling rate was 500 Hz. The EEG was filtered online with a low cut off filter of 0,1 and a high cut off filter of 100 Hz and referenced to the vertex electrode. Electro-oculogram (EOG) was recorded with four electrodes located below and lateral to eyes. Electrode impedances were pursued to set below 50 kΩ in the beginning of the experiment. During the experiment, the quality of the data was monitored and the electrode impedances were adjusted when necessary.

Averaging. The data was pre-processed and averaged using BESA 5.1 analysis program (http://www.besa.de/). The EEG was digitally filtered off-line with a low cut off filter of 0.53 Hz using a 6 dB/octave roll off and a filter type forward. To attenuate electrical noise, notch filter was set to 50.0 Hz with the width of 2.0 Hz. Eye blinks in the data were corrected before averaging with an individual eye blink correction algorithm implemented in BESA using PCA (Ille, Berg & Scherg, 2002). Responses to all speech stimuli in the oddball and in the equal probability conditions were averaged separately in epochs of -300 – 1070 ms and baselined to

-50 - 0 ms. Channels with multiple artefacts throughout the data were set bad and omitted from the averaging. Artefactual epochs with the voltage deflections exceeding ±150 μV peak-to-peak were also excluded from the averaging. For the stimuli of interest in this study, the mean number of epochs accepted for averaging was 93 for pre-deviant *standard-/atta/* (range 69-114) and 56 for *EQ-/atta/* (range 47-65). After the averaging, the channels previously set as bad channels were interpolated using spherical spline interpolation method (Perrin et al., 1989) and the data was filtered with a zero phase high cut off filter of 35 Hz using a 12 dB/octave roll off.

Current source density (CSD) transformation. Averaged ERPs were also transformed into CSD waveforms with BESA using CSD-Laplacian (10-10) montage resulting in interpolation to standard 81 channels. BESA computes the CSD waveforms as a second spatial derivative by spherical spline interpolation using information from all electrodes. A more detailed description of this method can be found in Perrin et al. (1989).

2.4. Data analysis

In this study, the analyses were guided by the prior knowledge in the literature of the N1 sub-components and the latency range of their occurrence. The analyses were restricted only to the responses to /atta/-stimulus based on inspection of the grand averaged ERP waveforms, which revealed that longer silent gap in the stimulus allowed the waveform to develop better with less overlap with the responses to the second syllable. The /atta/-stimulus was chosen because it enabled the investigation of the brain responses to the same stimulus presented frequently with a fast ISI in an oddball paradigm and rarely with a longer ISI in an equal probability paradigm. In this study, the responses to pre-deviant standard-/atta/ and to EQ-/atta/ were analysed. Because the main interest of this study was in the method used to analyse the data, the dataset was predefined to be as simple and unambiguous as possible in order to facilitate the interpretation of ICA analysis. For this purpose, the inspection of the data was further restricted only to the responses to the first vowel /a/ of the /atta/-stimulus in order to exclude overlapping responses to the first and the second syllable.

ICA analysis. Independent component analysis was performed using EEGLAB 5.04, a freely available open source toolbox (http://www.sccn.ucsd.edu/eeglab) developed by Delorme and Makeig (2004), running under Matlab 7.0.1 (www.mathworks.com). The average-referenced

ERP average waveforms of all speech stimuli and their reference-free CSD transformations were imported to EEGLAB. Two separate datasets were created, one for ERP waveforms and one for CSD waveforms, both including the responses to all speech stimuli from 20 participants. Even though the analysis were chosen to concentrate only to the responses to the first syllable /a/ of the /atta/ stimulus, all the speech stimuli were used as an input to ICA analysis to increase the input-to-timepoint ratio of the data to the sufficient level suggested by Onton et al. (2006). ICA was performed to epochs of -50 to 855 ms of both average reference ERP and reference free CSD datasets, resulting in the same number of components as there were channels in the input data; 128 for ERP and 81 for CSD datasets. ICA learning batch size was 58 samples. Initial learning rate started at 0.001 and was gradually reduced to 1E-7 during 373 learning iterations for ERP and 362 for CSD. In the next step, after applying ICA to ERP and CSD datasets including the responses to all speech stimuli, the attained component weightings were applied separately only to the responses to the first syllable and the voiceless stop of the pre-deviant standard- and EQ-/atta/.

ICA component selection. The resulting ICA solutions, ERP-ICA and CSD-ICA, were explored to identify N1 components activating in response to the first syllable /a/ in the EQ- and standard-/atta/ conditions. A large number of components returned by ICA, when applied to multi-channel data, makes it challenging to decide which of the components are of interest and which represent artefactual sources. In this study, the components of interest were identified by visual inspection of topographical 2-D and 3-D scalp maps of the components and their activation time courses. The selection of the N1-ICA components was driven by the theory of activation of N1 and its sub-components in children.

The N1 was expected to activate more profoundly in long ISI condition, and thus the ICA components of interest were selected based on their activation in response to EQ-/atta/. The activation of the selected ICA components were inspected also in response to standard-/atta/. This was done in order to see whether the same N1-ICA components activated in the short ISI condition too, even though the N1 was not clearly visible from the grand averaged waveforms elicited with the short ISI. In order for a component to be selected for further inspection, the activation time course of the component had to show activity during the expected latency in response to EQ-/atta/ and the distribution of the component scalp map had to be in line with the theory.

The component types that were searched for were: 1) N1a, a radial temporal negativity at the left hemisphere around 75 ms (Bruneau & Gomot, 1998), 2) a frontal negativity around 110 ms (Bender et al, 2006), 3) N1b, a frontocentral or parietal negativity accompanied with temporal positivities around 110 ms reflecting activation in the supratemporal plane (Bruneau & Gomot, 1998; Hämäläinen et al, 2007; Näätänen & Picton, 1987; Pang & Taylor, 2000; Ponton et al, 2002), 4) Ta, bilateral radial temporal positivity around 110 ms (Ponton et al., 2002; Tonnquist-Uhlen et al, 2003), 5) non-specific N1, a vertex-negativity around 130 ms (Hari et al., 1982; Karhu et al., 1997; Näätänen & Picton 1987), 6) a frontal negativity around 140-150 ms (Bender et al., 2006), and 7) N1c, a radial temporal negativity around 170 ms (Bruneau & Gomot, 1998; Pang & Taylor, 2000). (For a more detailed description of the N1 sub-components, see the Introduction.) The selection of ICA components of interest was carried out separately for ERP and CSD datasets. It was expected, that due to an inevitable intersubject variability, the strengths of different ICA component scalp maps and activation time courses would vary across participants and different participants would contribute to different ICA components. Thus, not every participant was expected to contribute to every component. Instead, several similar sub-components contributed by sub-group of the participants were expected to be decomposed.

In the next step, the selected ICA components were grouped together to form clusters of similar components. The component clusters were created by visual inspection based on similarities of ICA component 2D and 3D scalp maps and activation time courses, assuming that similar components represent analogous underlying brain activity. Also the contribution of participants to the components was assessed to find out how many participants contributed to which component. One component could be assigned into several clusters according to it's activity in different time windows. Clustering was performed separately for ERP-ICA and CSD-ICA resulting in two separate sets of clusters. Source localization would also have been helpful in the selection and clustering of ICA components of interest, but it could not be applied in the scope of this master's thesis.

3. RESULTS

Next, brain responses of 20 healthy 9-year-old children to EQ-/atta/, presented with equal probability with a long ISI varying pseudo-randomly between 1 -5 seconds, and to standard-/atta/, presented as a standard in an oddball paradigm with a short ISI of 610 ms, are

presented. Figures 1 and 3 present grand averaged ERP and CSD waveforms while figures 2 and 4 show 2-D topography maps of the grand averaged ERP and CSD waveforms in the latency range of 75 to 175 ms.

3.1. Visual inspection of grand averaged ERP waveforms and topographies

Figure 1 shows grand averaged ERP waveforms of the responses to EQ- and standard-/atta/ at selected channels. At central channels (C3, Cz, C4), the response to first syllable /a/ of EQ-/atta/ showed clear P1, N1, P2 and N2 peaks while the response to first syllable /a/ of standard-/atta/ consisted of a positive P1-N1-P2 –wave and a large N2 peak. Reversal of the polarity can be seen at temporal (T3, T4) and mastoid channels (ML, MR). At central channels, the N1 to EQ-/atta/ peaked at the latency of 110 ms whereas the N1 to standard-/atta/ peaked only as a small deflection from the positive wave at 116 ms. The amplitude of the N1 to standard-/atta/ was markedly more positive than in response to EQ-/atta/. A large P2 peaked in response to EQ-/atta/ at the latency of 190 ms. The N2, on the other hand, was larger in response to standard-/atta/ and also peaked earlier in latency of 260 ms while the N2 in response to EQ-/atta/ peaked at 290 ms.

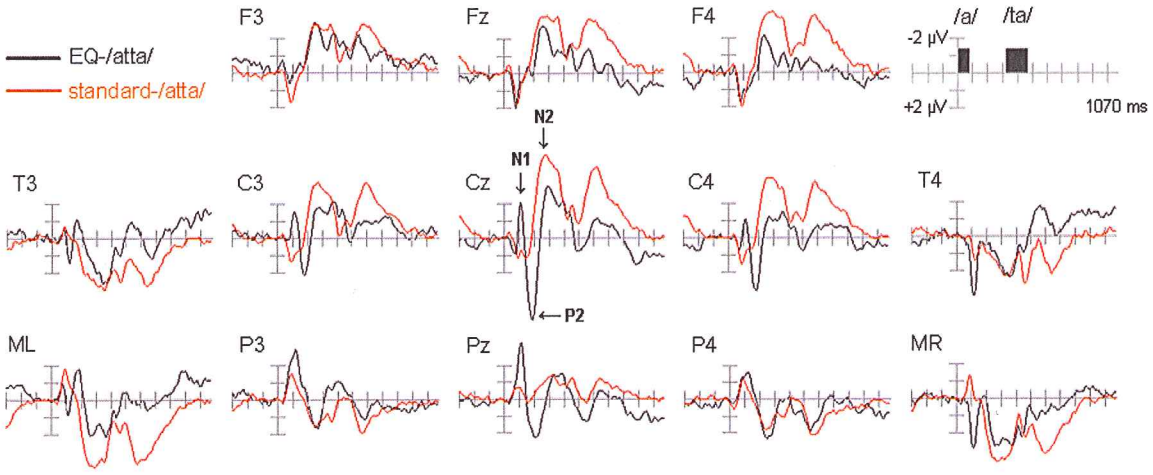

Figure 1. Grand averaged ERP waveforms in response to EQ-/atta/ (black line) and standard-/atta/ (red line) at the latency range of -300 - 1070 ms on selected channels (frontal: F3/E25, Fz/E11, F4/E124; central: C3/E37, Cz/E129, C4/E105; parietal: P3/E60, Pz/E62, P4/E86; temporal: T3/E46, T4/E109; mastoid: ML/E57, MR/E101; 10-20 system electrode numbers/EGI 128-sensor net electrode numbers).

Figure 2 shows 2-D topographies of the grand averaged ERP waveforms during the N1 time window in the latency range of 75 - 175 ms. In *response to EQ-/atta/* (Fig. 2, left panel), a negativity was distributed around left temporal site and parietal areas at 65 ms where it shifted to more central site activating at centroparietal areas around 105 - 135 ms. Centroparietal negativity was accompanied with temporal positivities with a right hemisphere dominance. Around 145 - 165 ms, negativities were observed at temporoparietal areas, especially at the left hemisphere, and also at midfrontal site from 155 ms onwards. From 55 to 135 ms, the *response to standard-/atta/* (Fig. 2, right panel) was dominated by frontocentral positivity, while a negativity was observed over temporal (larger at the left hemisphere) and parietal areas. From 145 ms, the positivity moved to more central site and over right temporoparietal areas with the negativity withdrawing to left parietal area and finally disappearing at 175 ms. A frontal negativity appeared around 155 ms.

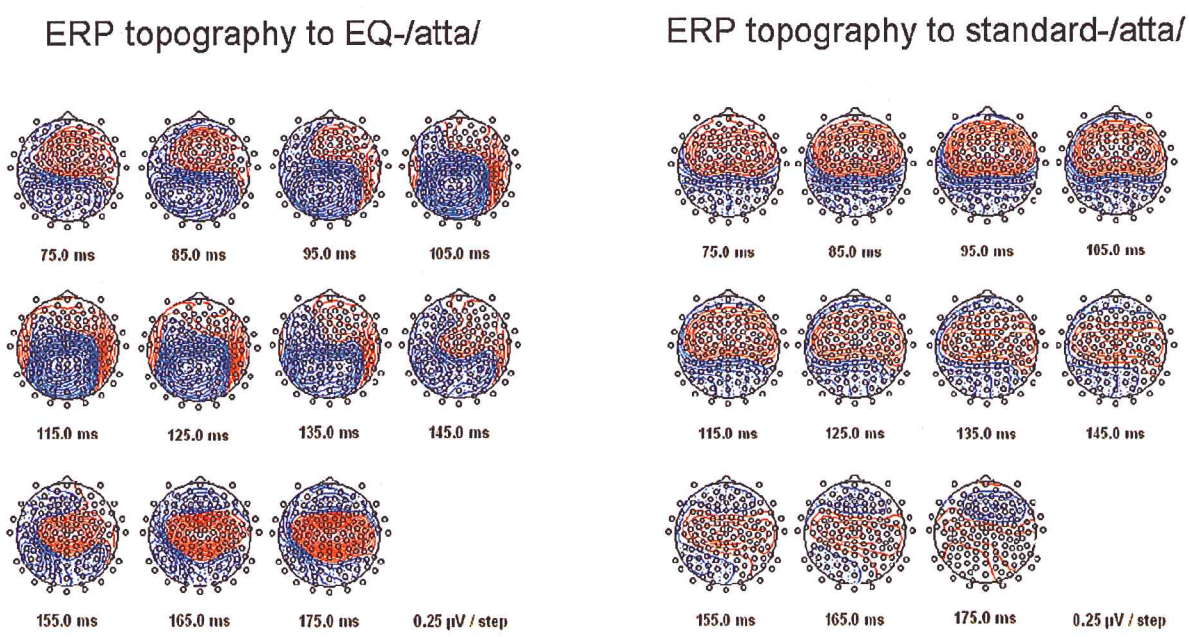

Figure 2. Topographies of the ERP grand averaged waveforms in response to EQ-/atta/ (left panel) and standard-/atta/ (right panel) at the latency range of 75 - 175 ms.

3.2. Visual inspection of grand averaged CSD waveforms and topographies

Figure 3 shows grand averaged CSD waveforms of the corresponding responses to EQ- and standard-/atta/ at the same selected channels. At central channels (C3, Cz, C4), the CSD response to first syllable /a/ of EQ-/atta/ showed P1, N1, P2 and N2 peaks while the CSD response to first syllable /a/ of standard-/atta/ consisted of a positive P1-N1-P2 –wave and a large N2 peak, as in ERP waveforms too. Reversal of the polarity can be seen at temporal (T3, T4) and mastoid (ML, MR) channels. In response to EQ-/atta/, N1-CSD peaked at central areas at the latency of 110 ms. Peaking at 110 ms as a small deflection from positive P1-N1-P2 wave, N1-CSD component to standard-/atta/ was markedly smaller than the N1-CSD to EQ-/atta/. Nevertheless, the difference in magnitude of the N1 component to standard- and EQ-/atta/ was not as large in CSD waveforms as was observed from the respective ERP waveforms. The P2-CSD peaking at central areas at 180 ms was larger in response to EQ-/atta/. The N2-CSD peak in response to EQ-/atta/ peaked at central channels at 290 ms while N2-CSD to standard-/atta/ peaked earlier at 270 ms being slightly larger in amplitude.

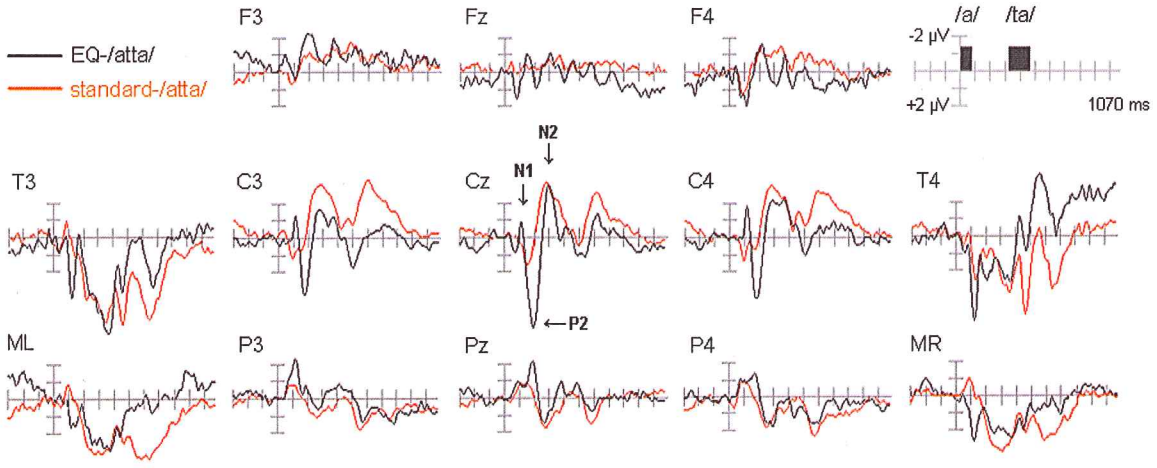

Figure 3. Grand averaged CSD waveforms in response to EQ-/atta/ (black line) and standard-/atta/ (red line) at the latency range of -300 - 1070 ms on selected channels (frontal: F3/F3, Fz/Fz, F4/F4; central: C3/C3, Cz/Cz, C4/C4; parietal: P3/P3, Pz/Pz, P4/P4; temporal: T3/T7, T4/T8; mastoid ML/TP9, MR/TP10; 10-20 system electrode numbers/10-10 system electrode numbers).

Figure 4 shows 2-D topographies of the grand averaged CSD waveforms during the N1 time window in the latency range of 75 - 175 ms. In the CSD topographies, sources and sinks represent magnitude of radial current flow entering (sink) and leaving (source) the scalp (Nunez, 1981). (For a more detailed description of current source density method, see the Introduction.) In *response to EQ-/atta/* (Fig. 4, left panel), bilateral prefrontal sinks were active from 60 to 115 ms along with temporoparietal sinks (more temporal at the left hemisphere) that activated at 65 - 85 ms. Temporal sources (right larger than left) were active from 105 to 145 ms corresponding to bilateral centroparietal sinks that started to shift to temporoparietal areas after 125 ms reaching temporal areas at 155 ms. At 155 - 185 ms a midfrontal sink was observed. The *response to standard-/atta/* (Fig. 4, right panel) was dominated from 65 to 115 ms by bilateral frontocentral sources corresponding to frontal and temporoparietal sinks. At 145 ms a frontal sink appeared and the parietal negativity shifted to left parietal site.

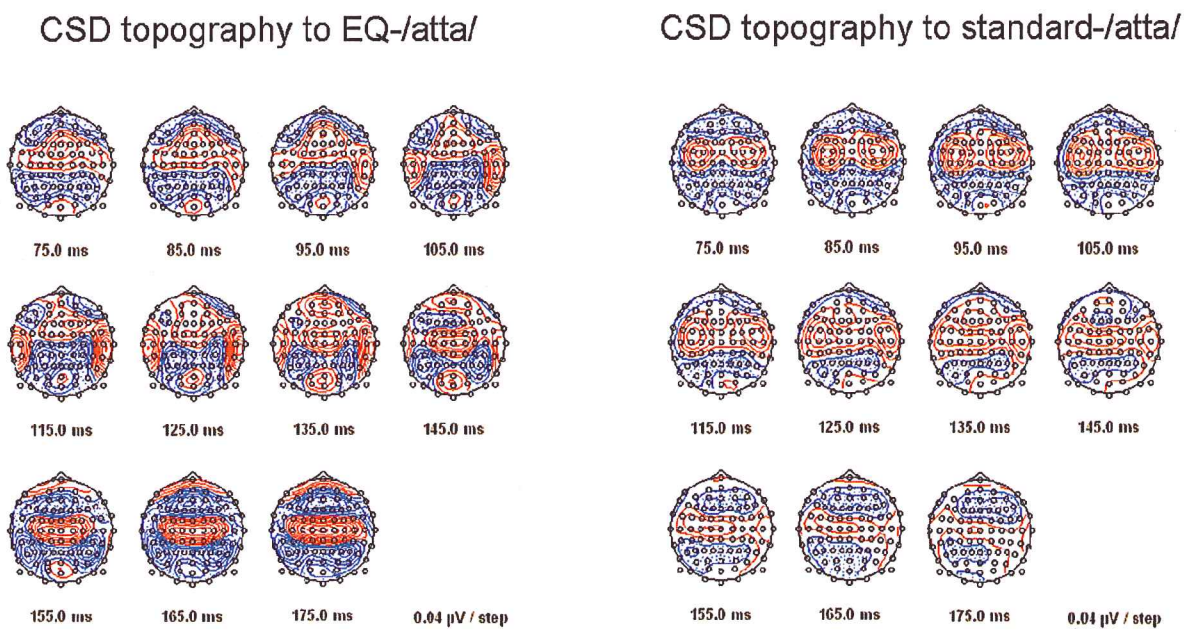

Figure 4. Topographies of the CSD grand averaged waveforms in response to EQ-/atta/ (left panel) and standard-/atta/ (right panel) at the latency range of 75 - 175 ms.

This study replicates the finding reported in several previous studies by demonstrating that N1 amplitude decreases as a result of shortening the ISI. The grand averaged ERP and CSD waveforms clearly indicate that N1 response to first syllable /a/ of /atta/-stimulus recorded from central channels is markedly more larger when the stimulus is presented with an equal probability and a long ISI in, and almost vanishes when the stimulus is presented as a standard with a shorter ISI in an oddball paradigm. In fact, just by looking the waveforms and topographies of ERP and CSD response to standard-/atta/, it is hard to determine whether the N1 actually is present in the data or not.

3.3. Identification of ERP-ICA and CSD-ICA N1 sub-components

ICA was performed separately to averaged ERP waveforms and their CSD transformations of all speech stimuli presented in the oddball and equal probability paradigms resulting in decomposition of 129 ERP-ICA components and 81 CSD-ICA components. In this study, the inspection of ICA components was restricted to N1-ICA components activating in responses to first syllable /a/ of EQ- and standard-/atta/ stimuli. ICA components of interest were selected on theoretical grounds based on visual inspection of their topographical scalp distribution maps and their temporal activation in the long ISI condition. Clustering was performed separately for ERP-ICA and CSD-ICA.

Next, N1-ICA component clusters to the first syllable /a/ of EQ- and standard-/atta/ decomposed from averaged ERP and CSD waveforms are presented. The figures present topographical scalp maps of the selected ICA components and their temporal activation patterns in response to EQ- and standard-/atta/. The scalp map of each ICA component is identical at each time point of the component's temporal activation pattern, apart from its magnitude, which is scaled according to the temporal activation value at each time point and reversed when temporal activation pattern is negative. For clarity, in the figures here, whenever the temporal activation pattern of a component is negative during the time window of interest, the corresponding component scalp map is depicted inverted, as indicated by the sign '-' in front of the component number. The activation peak latencies at N1 time window of the selected components and the number of participants contributing to the components are presented in Tables 1 and 2 in response to both EQ- and standard-/atta/.

During the N1 time window, a total of 24 ERP-ICA and 19 CSD-ICA components showed activation in response to first syllable /a/ of EQ-/atta/ stimulus presented with long ISI. These components were grouped into 8 ERP-ICA and 6 CSD-ICA clusters based on the similarities of their scalp distribution maps and temporal activation patterns. Two ERP-ICA components and seven CSD-ICA components were assigned into two clusters.

N1a, temporal negativity. Figure 5 presents an ERP-ICA cluster activating at temporal areas around 80 ms (ERP-T80). The ERP-T80, decomposed from ERP waveforms, consisted of two components that had radial temporal negativities at the left hemisphere. The independent component number 74, with inverted scalp map, decomposed from ERP waveforms (IC -E74) showed some activation also at the right temporal hemisphere, but the left hemisphere activity was clearly dominating. The ERP-T80 activated around 80 ms in response to both EQ- and standard-/atta/ showing somewhat larger activation in the long ISI condition.

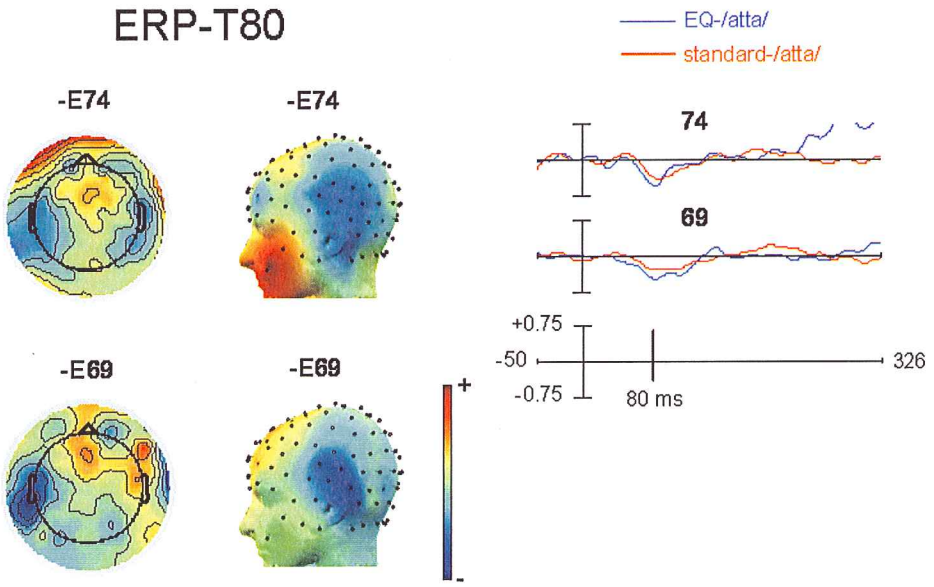

Figure 5. Scalp maps and temporal activation patterns of the ERP-ICA components constituting the cluster ERP-T80 activating at temporal areas around 80 ms.

Figure 6 presents a CSD-ICA cluster activating at temporal areas around 84 ms (CSD-T84). The CSD-T84 was composed of four early activating components, decomposed from CSD waveforms, that had radial sinks at the left temporal hemispheres. The independent component number 24 decomposed from CSD waveforms (IC C24) activated also slightly at the right hemisphere, but the main activation was at left temporal site. The IC C14 had a concurrent frontal sink at the right hemisphere while the ICs C59 and -C60 had concurrent midparietal sinks. The only component activating in response to standard-/atta/ was the IC C24, which was, however, contributed by only four participants (see Table 2).

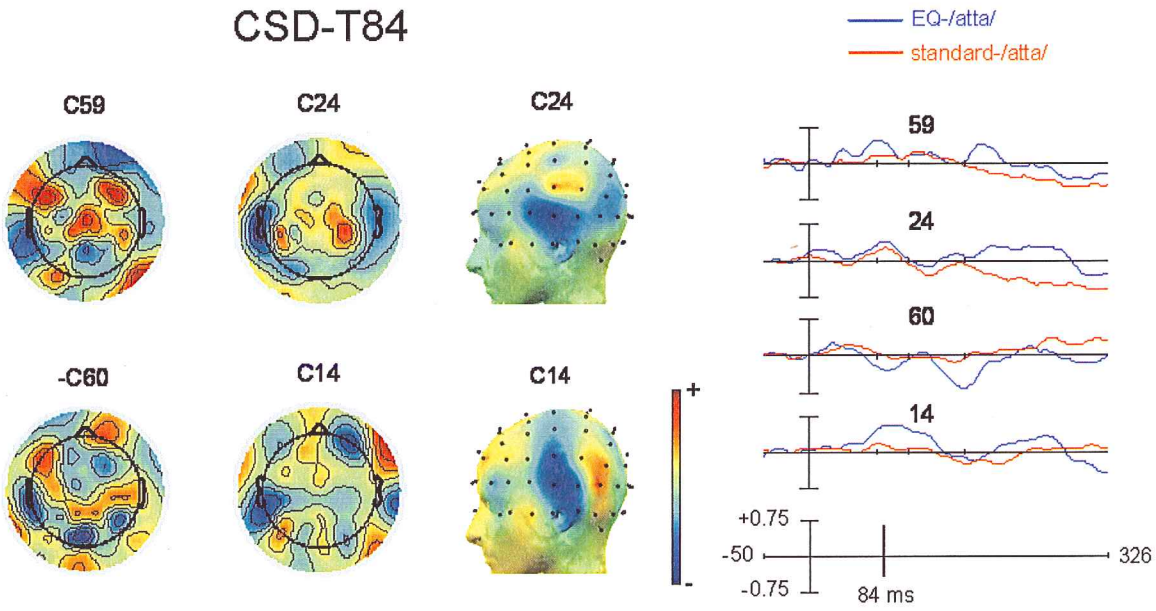

Figure 6. Scalp maps and temporal activation patterns of the CSD-ICA components constituting the cluster CSD-T84 activating at temporal areas around 84 ms.

Ta, temporal positivity. Cluster of components with radial temporal positivities decomposed from ERP waveforms is presented in Figure 7. Cluster ERP-T112 was composed of ERP-ICA components that showed positive radial temporal activation around 112 ms. One of the components in ERP-T112, IC -E83, had bilateral radial temporal positivity while the other four components showed radial positivity only at the right temporal hemisphere. Interestingly, components showing some negative activity at the left temporal hemisphere in response to EQ-/atta/, ICs -E19 and -E21, also activated slightly during the time window of ERP-T80 which accounted for the negativity at the left temporal hemisphere around 80 ms. However, the left temporal negativities in these components were not as focal and radial looking as in the ERP-T80 components. The right hemisphere radial temporal positivities of the ICs -E19 and -E56 showed activation also in response to standard-/atta/ while the other components activated only in long ISI condition.

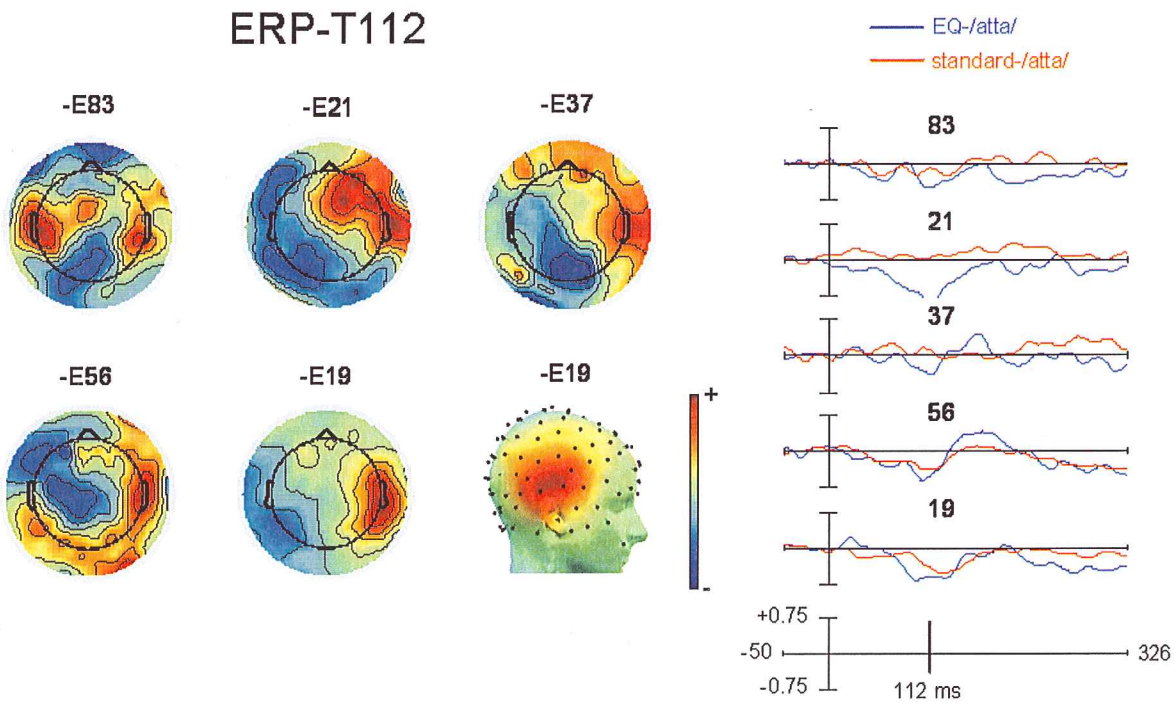

Figure 7. Scalp maps and temporal activation patterns of the ERP-ICA components constituting the cluster ERP-T112 activating at temporal areas around 112 ms.

Figure 8 presents the cluster of components with radial temporal sources decomposed from CSD waveforms. CSD-ICA components, with radial temporal sources in both or only one hemisphere, formed the cluster CSD-T107 that activated around 107 ms. Most of the components, ICs C73, C63 and -C26, activated also at N2 time window. The structure of IC -C3 might also have been dipolar but the possible dipole seemed to be too superior to be generated by tangential source in supratemporal plane and thus the component was assigned into the radial temporal cluster. The IC C3 also activated with reversed scalp distribution at the later N1c latency in response to both EQ- and standard-/atta/ and also at the earlier N1a latency in response to standard-/atta/. Only one CSD-T107 component, IC C73, activated at the Ta time window in response to standard-/atta/.

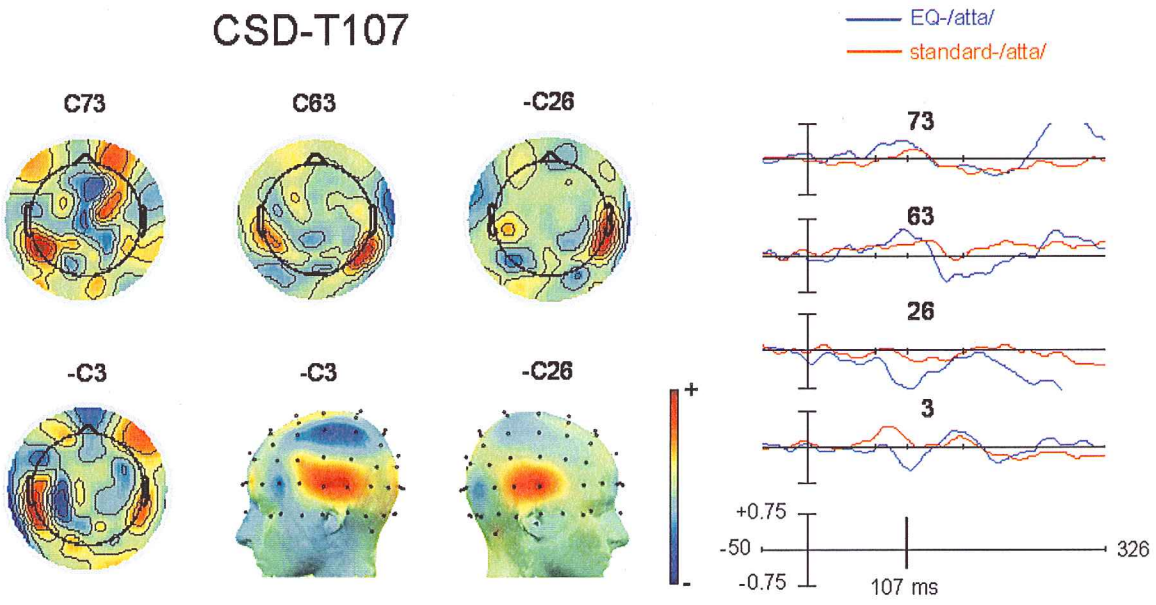

Figure 8. Scalp maps and temporal activation patterns of the CSD-ICA components constituting the cluster CSD-T107 activating at temporal areas around 107 ms.

Parietal negativity. ERP-ICA cluster ERP-P112 is presented in Figure 9. The ERP-P112 consisted of four components composed of negativities at parietal areas and accompanying positivities at frontal sites. ICs -E46 and -E23 had large activations peaking at 112 ms. ICs E41 and E100, peaking earlier in latency, were contributed by only a few participants (see Table 1) and their activations were also notably weaker. In response to standard-/atta/, only ICs E41 and E100 were active. No CSD-ICA components having only parietal distribution activated around this time window. Nevertheless, in some CSD-ICA components, parietal sinks were associated with other concurrent activity elsewhere in the brain, but these components were assigned into other clusters according to the leading activity of the component.

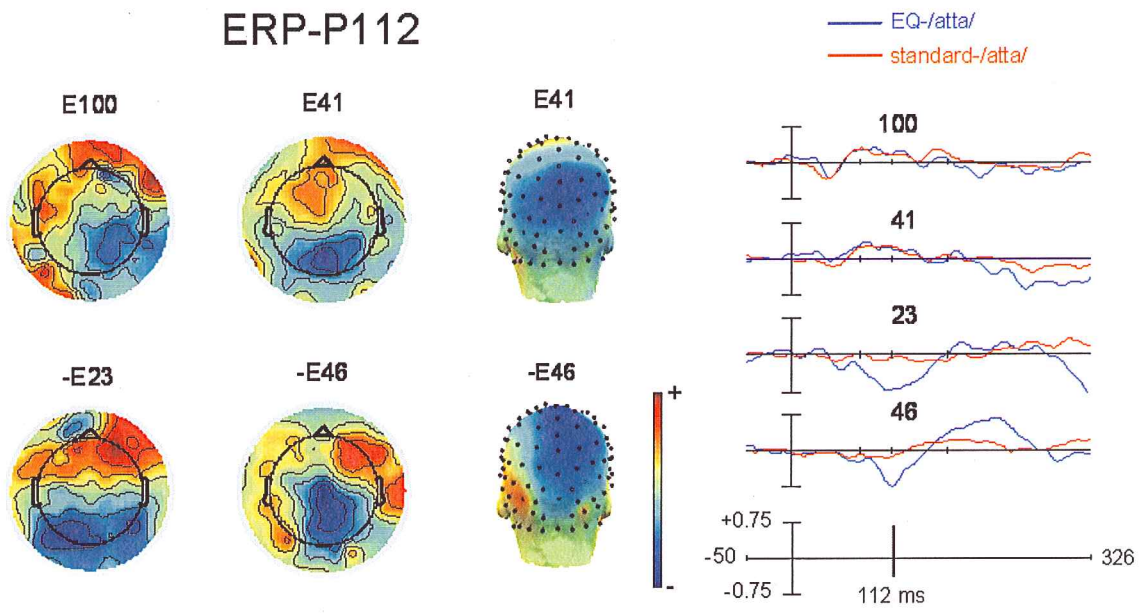

Figure 9. Scalp maps and temporal activation patterns of the ERP-ICA components constituting the cluster ERP-P112 activating at parietal areas around 112 ms.

Frontal negativity. Frontal components assigned to clusters ERP-F114 are presented in Figure 10. ERP-F114 consisted of one ERP-ICA component that had a negative distribution over frontocentral scalp site. It activated only in response to EQ-/atta/ around the latency of 114 ms, but only in 6 participants (see Table 1). It showed somewhat larger activation with inverted topography around P2 time window as well. No other frontal components activating around the same time window were decomposed from ERP waveforms in response to EQ -/atta/.

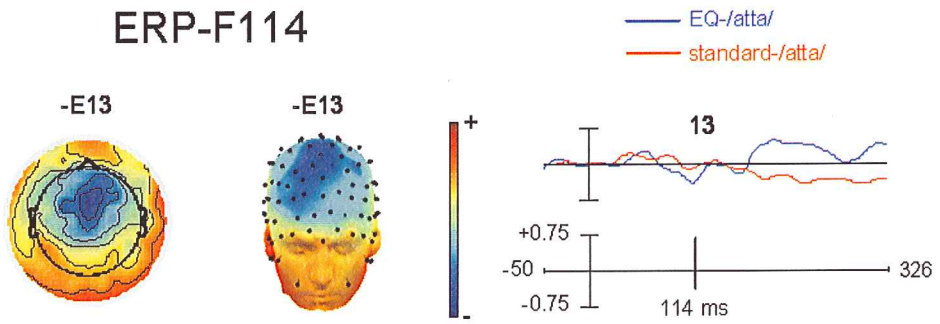

Figure 10. Scalp maps and temporal activation patterns of the ERP-ICA components constituting the cluster ERP-F114 activating at frontal areas around 114 ms.

Figure 11 presents the CSD-F110 cluster activating at frontal areas around 110 ms. Several CSD-ICA components with frontal distribution activated around the latency of 110 ms in response to EQ-/atta/. Four of the CSD-ICA components in CSD-F110 cluster had bilateral prefrontal or frontal sinks whereas one component had a frontal sink only at the right hemisphere and two of the components were composed of midfrontal sinks. ICs -C9 and -C13 activated also for N2 and IC -C6 with inverted topography for P1 and P2. Three of the CSD-F110 components also activated in response to standard-/atta/ at somewhat earlier latency (see Table 2).

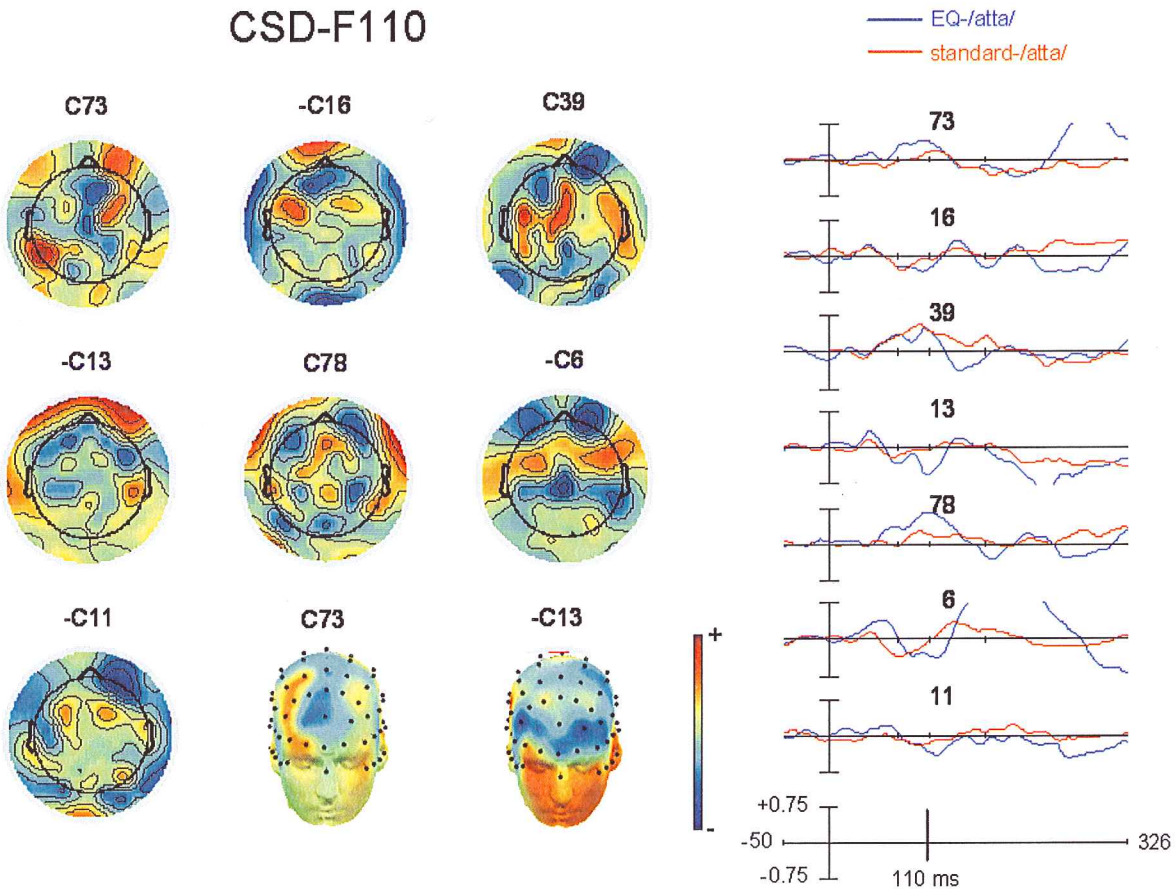

Figure 11. Scalp maps and temporal activation patterns of the CSD-ICA components constituting the cluster CSD-F110 activating at frontal areas around 110 ms.

N1b, supratemporal negativity. Figure 12 presents the ERP-ST116 cluster which consists of components decomposed from ERP waveforms. ERP-ST116 components that had broad negativities distributed over central areas and accompanying positivities at temporal or temporoparietal areas activating around the latency of 116 ms. The reversal of the polarity

occurred over the Sylvian fissure, suggesting a tangential source located in the temporal lobe. ICs E8, E2, E9, -E7 and -E4 showed very similar structure. Activation of ICs E8, E2 and E9 was notably weaker than the activations of the rest of the components in the ERP-ST116 around the latency of 116 ms. While the abovementioned components activated at both hemispheres, IC -E15 activated at the right hemisphere and IC E39 at the left hemisphere. The components in the ERP-C116 cluster did not activate during the N1 latency range in response to standard-/atta/. Instead, in the short ISI condition, ICs E8, E2, E9, -E7 and -E4 seemed to activate at the later latency of N2 time window and ICs -E7 and -E4 also with reversed scalp distribution around the P1 time window. In response to EQ-/atta/, many of the ERP-ST116 components activated also for N2 (ICs -E8, E9 and -E7) and with inverted scalp distribution for P1 (IC -E4) and P2 (ICs E8, -E15).

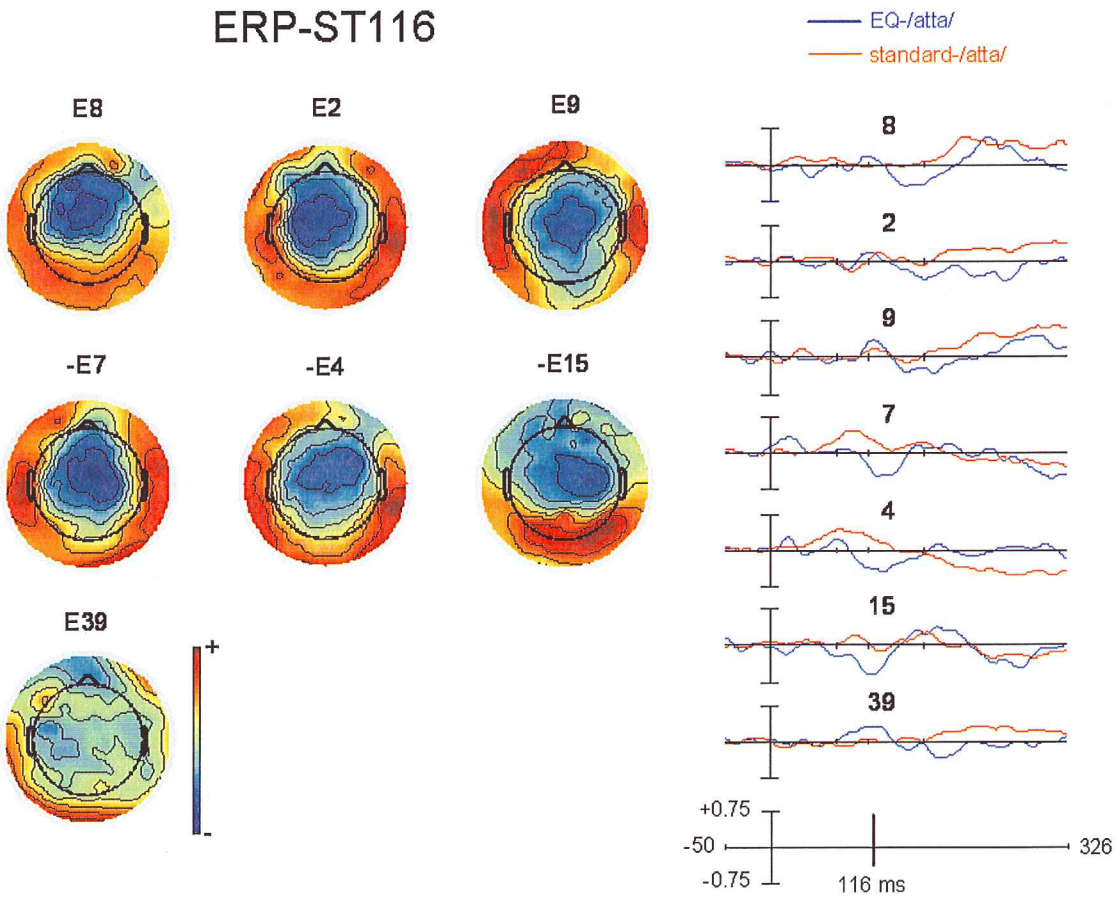

Figure 12. Scalp maps and temporal activation patterns of the ERP-ICA components constituting the cluster ERP-ST116 activating around 116 ms.

Figure 13 presents the CSD-ST114 cluster which consisted of four CSD-ICA components activating in response to EQ-/atta/ around the latency of 114 ms. Less CSD-ICA components than ERP-ICA components reflecting activation of supratemporal N1b was identified. The components in CSD-T114 were composed of sources at temporal or temporoparietal areas that corresponded to sinks at central areas. The reversal of polarity over the Sylvian fissure indicated that the components were produced by tangential source located in the temporal lobe. IC C2 activated only at the right hemisphere, while the distributions of the other components were bilateral. In addition to tangential temporal activation, IC C78 had also bilateral frontal sinks and a midparietal sink. The CSD-T114 components in response to EQ-/atta/ activated only at N1 time window. In response to standard-/atta/, however, they did not activate at all during the N1 time window, but instead two of the components, ICs C2 and C1, activated for N2 and IC C1 also for P1 with inverted topography.

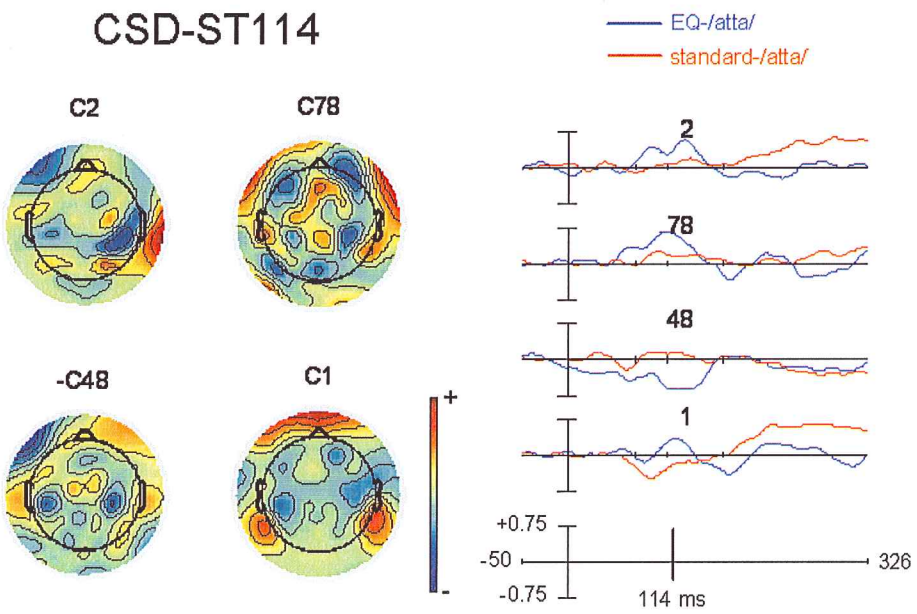

Figure 13. Scalp maps and temporal activation patterns of the CSD-ICA components constituting the cluster CSD-ST114 activating around 114 ms.

The scalp topography maps of the selected representative ERP-ST116 and CSD-ST114 components reveal that CSD-ICA component distribution was considerably more focused and localised than the distribution of the ERP-ICA component (see Figure 14).

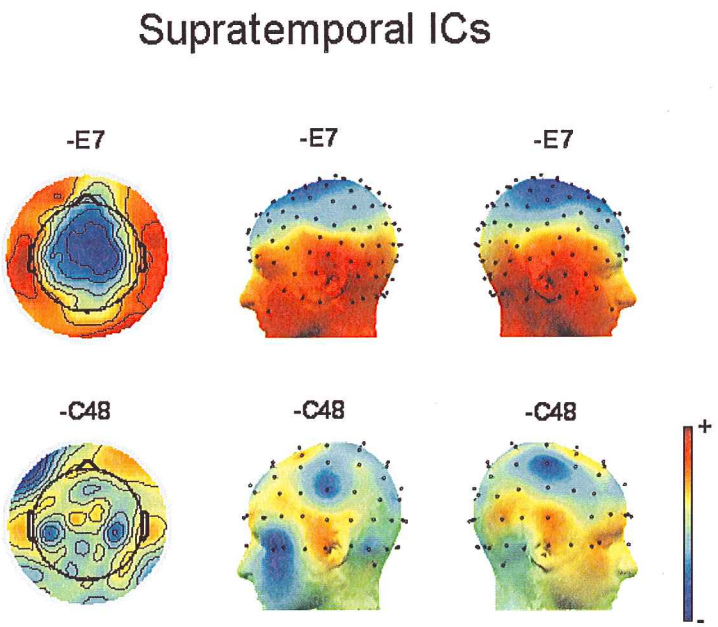

Figure 14. Scalp topography maps of the selected representative supratemporal ERP-ICA and CSD-ICA components.

Non-specific N1, vertex negativity. Figure 15 shows activation of two ERP-ICA components forming the cluster ERP-V127 activating around 127 ms. IC -E6 had centroparietal distribution centred around vertex, while IC -E75 activated at slightly posterior regions. The main activation of these components was, nevertheless, at P2 time window where they activated with reversed scalp distributions. Neither of these ERP-ICA components activated in response to standard-/atta/. Furthermore, no corresponding components activating at the non-specific N1 component time window were decomposed from CSD waveforms in response to EQ-/atta/. CSD-ICA component IC -C6 from cluster CSD-F110 (see Figure 11), however, had, in addition to prefrontal sinks, also a sink around the vertex, but it activated already around 118 ms.

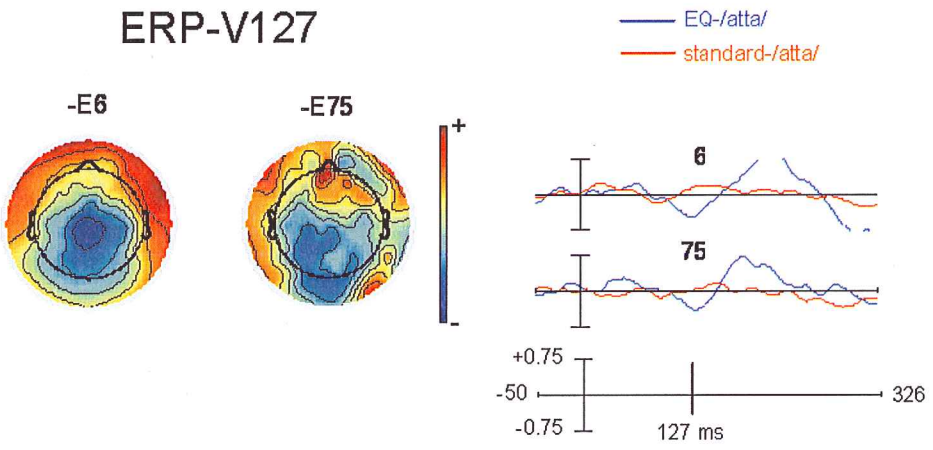

Figure 15. Scalp maps and temporal activation patterns of the ERP-ICA components constituting the cluster ERP-V127 activating at centroparietal areas around 127 ms.

Non-specific N1, frontal negativity. ERP-ICA and CSD-ICA clusters composed of frontal components activating around 140 ms are presented in Figures 16 and 17. ERP-F140 consisted of a single ERP-ICA component, IC -E10, that activated at 140 ms as a negativity over frontocentral area. CSD-F142, on the other hand, was composed of two components having either a midfrontal or bilateral frontal sinks that activated around 142 ms. None of these frontal ERP-ICA or CSD-ICA components activated at N1 time window in short ISI condition in response to standard-/atta/. However, the IC -E10 in ERP-F140 activated at the N2 time window in response to standard-/atta/.

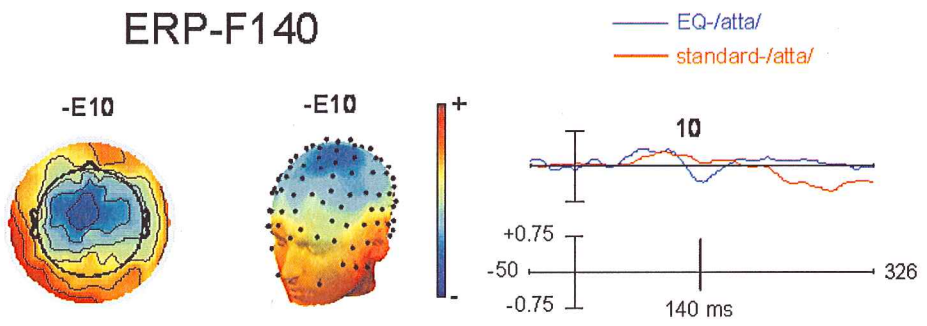

Figure 16. Scalp maps and temporal activation patterns of the ERP-ICA components constituting the cluster ERP-F140 activating at frontal areas around 140 ms.

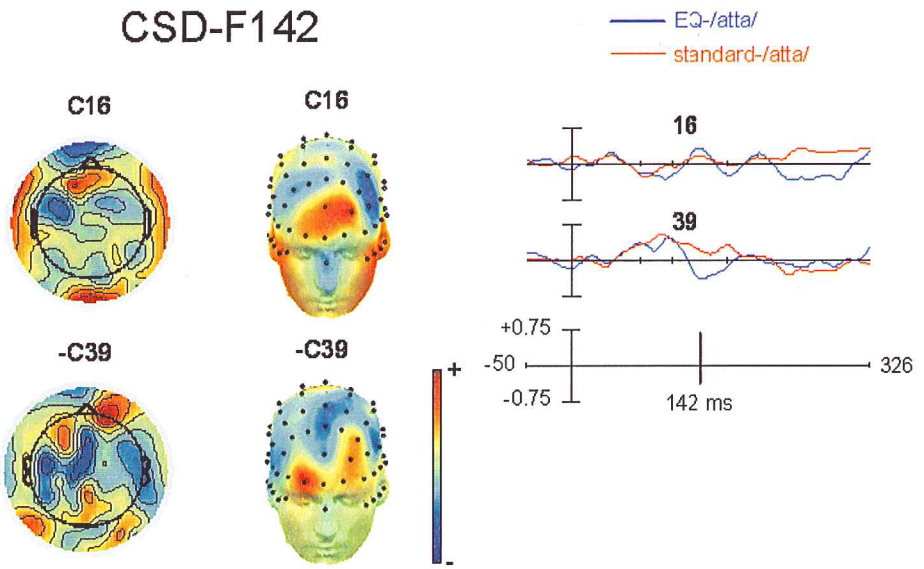

Figure 17. Scalp maps and temporal activation patterns of the CSD-ICA components constituting the cluster CSD-F142 activating at frontal areas around 142 ms.

N1c, temporal negativity. Figure 18 presents the ERP-ICA cluster representing late-latency temporal negativity. Cluster ERP-T163 was composed of four ERP-ICA components activating negatively around 163 ms at temporal areas. ICs -E91 and E114 had negativities at the left hemisphere, while ICs E37 and E56 had negativities at the right hemisphere. ICs E37 and E56 activated also earlier in latency with reversed scalp distribution belonging to temporal positivity ERP-T112 cluster. None of the components in ERP-T163 activated in response to standard-/atta/.

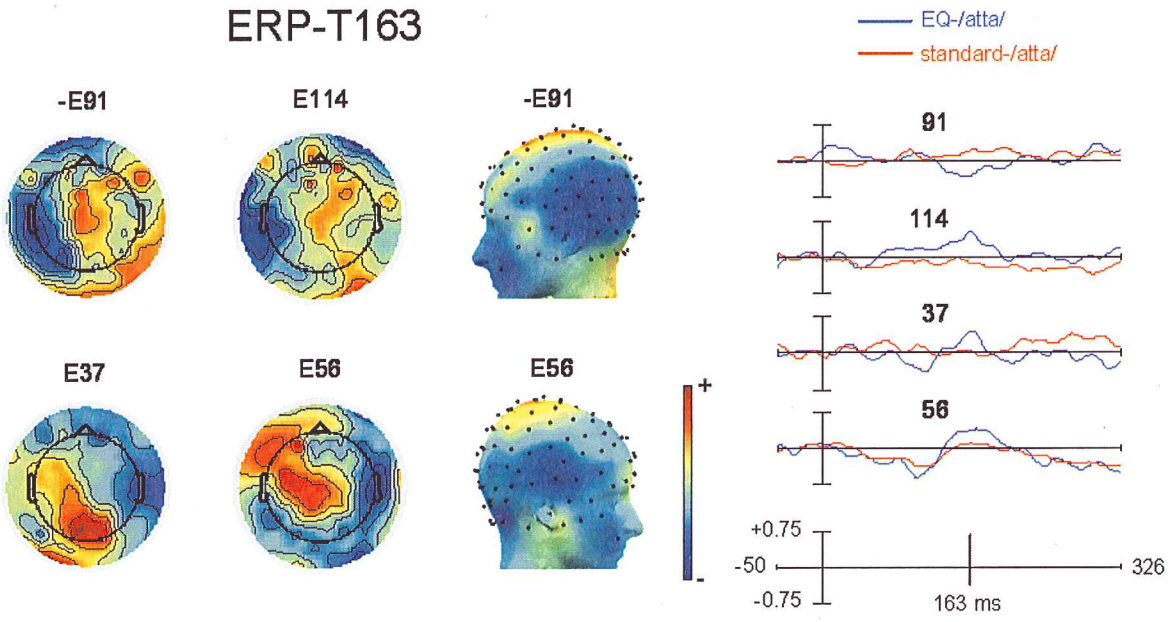

Figure 18. Scalp maps and temporal activation patterns of the ERP-ICA components constituting the cluster ERP-T163 activating at temporal areas around 163 ms.

The CSD-ICA cluster representing late-latency temporal negativity is presented in Figure 19. CSD-T160 consisted of CSD-ICA components activating around 160 ms in response to EQ-/atta/. Some of the components in CSD-T160 had bilateral radial temporal sinks while others had a radial sink only in one hemisphere. Right hemisphere temporal sinks in ICs -C42 and -C15 were somewhat inferior compared to sinks in other CSD-T160 components. Only IC C3 with bilateral temporal sinks activated also in response to standard-/atta/. The temporal sinks in CSD-T160 components were more localized than the large temporal negativities in ERP-T163 components that encompassed the whole temporal lobe.

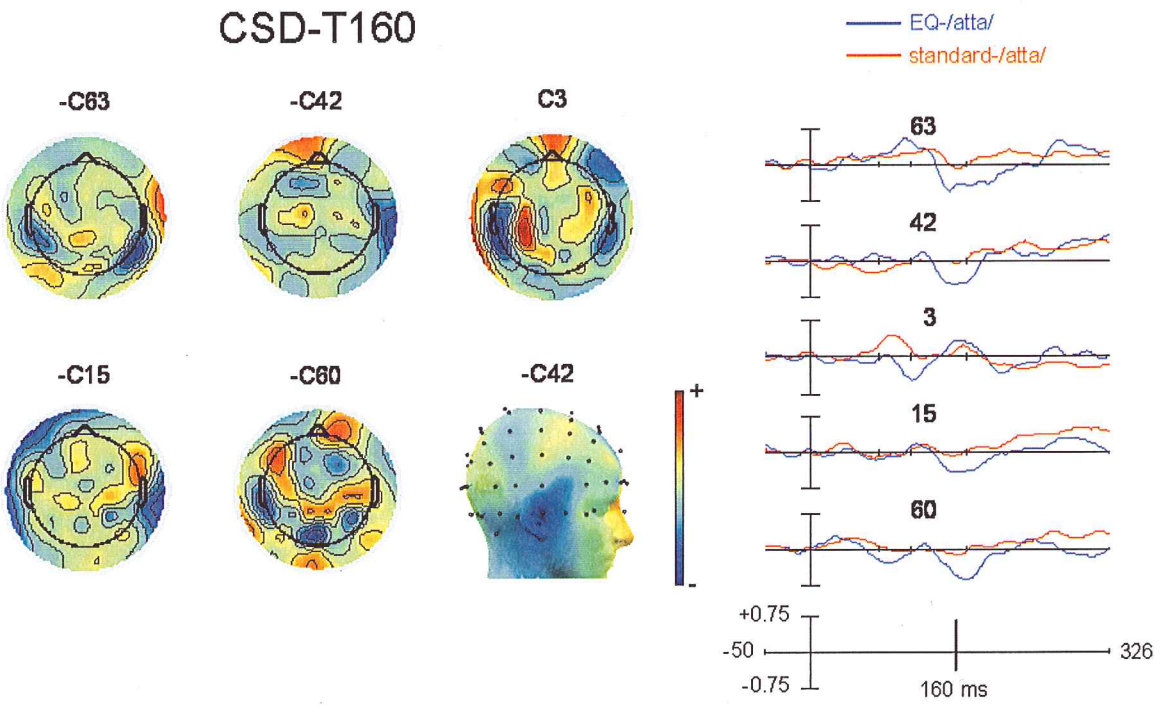

Figure 19. Scalp maps and temporal activation patterns of the CSD-ICA components constituting the cluster CSD-T160 activating at temporal areas around 160 ms.

ERP-ICA		EQ-/atta/		standard-/atta/	
Cluster	Component	Latency	Participants	Latency	Participants
ERP-T80	-E74	80	9	84	8
	-E69	80	6	90	6
ERP-T112	-E19	96, 128	8	126	8
	-E83	110	8	-	-
	-E21	112	10	-	-
	-E37	112	7	-	-
	-E56	116	9	112	7
ERP-P112	E100	80	6	76	6
	E41	82	5	92	7
	-E46	112	11	-	-
	-E23	112	9	-	-
ERP-F114	-E13	114	6	-	-
ERP-ST116	E8	108	8	-	-
	-E15	112	9	-	-
	E2	112	6	-	-
	E9	114	6	-	-
	E39	116	7	-	-
	-E7	120	9	-	-
	-E4	127	7	-	-
ERP-V127	-E6	127	6	-	-
	-E75	128	9	-	-
ERP-F140	-E10	140	10	-	-
ERP-T163	-E91	156	6	-	-
	E114	162	8	-	-
	E37	162	6	-	-
	E56	170	6	-	-

Table 1. ERP-ICA component peak activation latencies (in ms) and number of participants contributing to components activating at N1 time window in response to both EQ- and standard-/atta/.

CSD-ICA		EQ-/atta/		standard-/atta/	
Cluster	Component	Latency	Participants	Latency	Participants
CSD-T84	C59	74	9	-	-
	C24	84	7	84	4
	-C60	86	4	-	-
	C14	90	8	-	-
CSD-T107	C73	100	6	116	6
	C63	104	9	-	-
	-C3	112	10	-	-
	-C26	112	8	-	-
CSD-F110	C73	100	9	-	-
	-C16	102	6	80	4
	C39	74, 106	8	98	6
	-C13	74, 108	12	-	-
	C78	68, 108	10	-	-
	-C6	118	7	76	8
	-C11	118	7	-	-
CSD-ST114	C2	90, 128	8	-	-
	C78	108	10	-	-
	-C48	114	9	-	-
	C1	118	9	-	-
CSD-F142	C16	140	7	-	-
	-C39	144	7	-	-
CSD-T160	-C63	152	6	-	-
	-C42	156	7	-	-
	C3	160	9	160	8
	-C15	164	9	-	-
	-C60	170	10	-	-

Table 2. CSD-ICA component peak activation latencies (in ms) and number of participants contributing to components activating at N1 time window in response to both EQ- and standard-/atta/.

4. DISCUSSION

The aim of this Master's thesis was to investigate the use of ICA in the analysis of averaged high-density ERP waveforms and their CSD transformations recorded from 20 healthy 9-year-old children. The aim was to decompose auditory N1 component into biologically plausible independent components reflecting N1 activation in different experimental conditions. Furthermore, it was investigated which approach, ERP-ICA or CSD-ICA, would lead to a better ICA decomposition of N1 sub-components. ICA was performed separately for averaged ERP waveforms and their CSD transformations. The resulting solutions, ERP-ICA and CSD-ICA, were explored in order to identify the N1-ICA components. The N1 was expected to activate more profoundly in a long ISI condition, and thus the N1-ICA components were selected based on their activation in response to the first syllable /a/ of /atta/ stimulus presented in an equal probability paradigm with ISI varying pseudo-randomly between 1 and 5 seconds. The activation of the selected ICA components were inspected also in response to standard-/atta/ presented in an oddball paradigm with short ISI of 610 ms. The ICA components representing N1 activation were identified by visual inspection separately for ERP-ICA and CSD-ICA. The selection of N1-ICA components was drive by the theory of activation and scalp distribution of N1 sub-components in children. The selected N1-ICA components were grouped together based on visual inspection to form clusters of similar components reflecting activation of different N1 sub-components. In the following sections, the activation and the distribution of grand averaged N1-ERP and N1-CSD peaks and the selected N1-ICA component clusters are discussed in relation to the literature following with a discussion of the ability of the studied ICA approaches to isolate the N1 sub-components into independent components.

According to the literature, the N1 is normally recorded largest at frontocentral areas (Bruneau & Gomot, 1998; McCallum & Curry, 1980; Näätänen & Picton, 1987) reflecting the activation of N1b component. In this study, instead, the N1 in response to EQ-/atta/, presented with an equal probability and a long ISI, seemed to appear in more posterior areas at centroparietal site as observed from ERP and CSD topographies. Some studies, however, have also reported more parietal N1b distribution in children (Daruna & Rau, 1987; Goodin et al., 1978; Pang & Taylor, 2000). Centroparietal negativity and accompanying temporal positivities were observed from both grand averaged ERP and CSD waveforms in response to EQ-/atta/ at the latency of 110 ms. The ICA decomposition of the ERP waveforms in response

to EQ-/atta/ produced supratemporal, frontal and parietal component clusters activating around the latency of expected N1b time window, whereas the decomposition of the CSD waveforms returned only supratemporal and frontal component clusters.

Supratemporal N1b. The scalp distributions of supratemporal components, belonging to the clusters ERP-ST116 and CSD-ST114, changed polarity over the Sylvian fissure indicating that they were produced by tangential sources. These clusters were thought to reflect the activation of N1b, produced by a tangential source located in the supratemporal plane of the auditory cortex, as described by Näätänen and Picton (1987). The orientation and localization of the dipoles producing the observed electrical fields was a lot easier to assess from CSD-ICA components than from broad scalp distributions of ERP-ICA components. In response to EQ-/atta/, presented with a long ISI, several supratemporal components with similar scalp distributions were decomposed from ERP waveforms, whereas the decomposition of CSD waveforms, on the other hand, yielded to extraction of fewer and more defined supratemporal components. This could imply that the supratemporal N1b activation distributed to several ERP-ICA components might have been contributed by sub-groups of participants, whereas the overlap between participants in CSD-ICA supratemporal components might have been larger. According to Ponton et al. (2002), the N1b first becomes identifiable with fast stimulation rate at the age of 9 years as a small inflection of the positive P1 wave. In line with Ponton et al. (2002), in this study, the N1b in response to standard-/atta/ presented with a short ISI was observed as a small inflection of the positive wave in grand averaged ERP and CSD waveforms. However, neither of the supratemporal clusters activated in the short ISI condition.

Furthermore, when observing N1b-ICA components decomposed from ERP waveforms, it was impossible to say whether they represented the activation of supratemporal source of the N1b only, or whether they might have included activation of possible radial frontal or vertex sources as well. In theory, if two sources are active at the same latency, ICA may capture them into a single component even if they occur in different locations of the brain (Delorme & Makeig, 2004; Luck, 2005a). On the contrary, topographies of the CSD-ICA N1b components clearly revealed that there were no radial vertex sources observable from the CSD-ICA components reflecting N1b activation. Frontal sinks, on the other hand, were observed to activate concurrently with a supratemporal source in one CSD-ICA N1b component.

Frontal component of N1b. Frontal sources have been suggested to be associated to N1b activity (Bender et al., 2006). Frontal ICA clusters ERP-F114 and CSD-F110 were observed to activate in response to EQ-/atta/ during N1b time window. Interestingly, this frontal activation was revealed with ERP-ICA as well, even though inspection of grand averaged ERP waveforms did not show any signs of frontal activation during the N1b time window. However, ERP-F114 was composed of only one frontal component that was contributed by only 6 participants. In contrast, several frontal CSD-ICA components activating at the N1b time window were identified in response to EQ-/atta/. In grand averaged CSD topographies, early bilateral frontal sinks were observed in response to both EQ- and standard-/atta/, and some of the CSD-F110 components activated in the short ISI condition too, but at earlier latency. The cluster ERP-F114, on the other hand, did not show activity in response to standard-/atta/. Frontal activation during N1b time window in response to both long and short ISI has been reported in adults (Alcaini et al.,1994; Giard et al., 1994). In the study of Bender et al. (2006), investigating the maturation of frontal component in children, only long ISIs were used, and thus there is no information of frontal activation in children with short ISI. The CSD results obtained here, nevertheless, indicate that frontal activation is elicited in children with short ISI too, and that its latency shortens with faster stimulation rate. According to the abovementioned study of Bender et al. (2006), frontal N1b components, observed from CSD waveforms, were nearly absent in children in age group of 6-11 years and became clearly evident only in 12-18-year-old adolescents. Contradictory to results obtained in this study, the frontal N1b component of Bender et al. (2006) was elicited at mid-frontocentral site, whereas in this study, the scalp distribution of frontal ICA components were more frontal. These topographical differences might indicate that the activation of frontal components may not yet be fully matured in 9-year-old children.

Parietal N1b. In this study, also parietal ICA components activating at N1b time window were observed. The parietal ERP-P114 cluster had an early onset and the activation was longer lasting than the activation of the supratemporal and frontal ERP-ICA clusters. No parietal cluster was decomposed from CSD waveforms, but some CSD-ICA components that were assigned into frontal or early temporal clusters showed concurrent activation in parietal areas as well. Some previous studies have reported parietal N1b activation in children. With long ISIs the N1b in 7-year-old children was seen in parietal areas (Daruna & Rau, 1987) and in 9-year-old children at centroparietal site (Hämäläinen et al., 2007). Parietal N1b has also been reported to be elicited with short ISI in 9-10 -year-old children (Pang & Taylor, 2000). In this study, in response to standard-/atta/ presented with short ISI, no parietal negativity was

observed from grand averaged ERP or CSD waveforms. Nevertheless, two parietal ERP-ICA components in the cluster ERP-P114 activated also in response to standard-/atta/, whereas the same was not true for CSD-ICA components having parietal activation.

Non-specific N1. The centroparietal N1 distribution to EQ-/atta/ in this study, could also be explained by long ISI in the equal probability paradigm, which would activate the non-specific N1 vertex component, thus shifting the N1 predominance to more posterior regions. According to Näätänen and Picton (1987), due to a long refractory period, the non-specific N1 component is elicited with ISIs over 4 seconds and observed as a negativity over the vertex. In this study, the non-specific N1 was assumed to be elicited only in the long ISI condition. A negativity over the vertex was observed from ERP grand averaged waveforms in response to EQ-/atta/ between 105 and 135 ms. During the same latency range, parietal sinks and corresponding temporal sources were observed in grand averaged CSD waveforms, while no equivalent sinks/negativities were observed in response to standard-/atta/ neither from grand averaged CSD nor ERP waveforms. Decomposition of ERP waveforms revealed a cluster ERP-V127 activating in response to EQ-/atta/ only. The cluster ERP-V127 was composed of two components with negative centroparietal distribution activating around the latency of 127 ms. In the study of Karhu et al. (1997) the non-specific N1 was seen in 9-year-old children at vertex at the latency of 130 ms. Thus, the cluster ERP-V127 can be thought to reflect the non-specific N1. However, no CSD-ICA components having sinks at vertex around 130 ms were identified. This could mean either that, despite the distributions of ERP-V127 components, the vertex activation was not present in the data after all, or that it might have been produced by a deep source, as suggested by Hari et al. (1982), or by a broad dipole layer, which would cause its activation to be vanished with CSD transformation. According to Srinivasan (2005), the activity of deep sources or broad dipole layers may not be capture d by CSD.

Frontal component of non-specific N1. It has been suggested that the non-specific N1 is contributed also by activation of frontal generators (Alcaini et al., 1994; Bender et al., 2006). The frontal components linked to the non-specific N1 are elicited with long ISI around the latency of 140-150 ms and they are demonstrated to be elicited mid-frontally already in 6-year-old children (Bender et al., 2006) and more frontocentrally in adults (Alcaini et al., 1994). In this study, two frontal ICA clusters, ERP-F140 and CSD-F142, were observed to activate in response to EQ-/atta/ only. ERP-F140 had a negativity distributed over frontocentral areas while sinks in CSD-F142 were more focused and localised at frontocentral site. These frontal ICA clusters did not activate in short ISI condition, despite the fact that late

frontal activation was observed after 155 ms from grand averaged ERP and CSD waveforms in response to standard-/atta/ as well. This might indicate that late frontal activation in these different conditions were produced by independent sources in the brain. Judging from temporal and spatial behaviour of the ERP-F140 and CSD-F142 clusters and their absence in short ISI condition, it could be argued that these clusters reflect the activation of the frontal component of the non-specific N1. CSD-ICA components in CSD-F142 activated also during N1b latency, but with reversed scalp distributions, showing more frontal activation in earlier latency. This could indicate that the frontal N1 components observed during the time windows of N1b and non-specific N1 originate from different brain areas.

Temporal T-complex. Temporal activation resembling T-complex was observable in grand averaged ERP and CSD waveforms. Both ERP-ICA and CSD-ICA approaches decomposed the temporal activation into N1a-, Ta- and N1c-ICA components.

Temporal negativity, N1a. An early temporal negativity was observed from grand averaged ERP and CSD waveforms around 75 to 85 ms at left temporal site while right temporal site remained positive, indicating activation of N1a component. The N1a activation in response to EQ-/atta/ was reflected in clusters ERP-T80 and CSD-T84 that had dominating radial temporal negativities at the left hemisphere. The activation of these N1a-ICA components elicited dominantly at the left hemisphere was in line with results of Bruneau and Gomot (1998). The temporal activation patterns observed from grand averaged ERP and CSD waveforms in response to standard-/atta/, however, were quite different from the ones obtained with long ISI. In response to standard-/atta/, temporal negativities were seen in grand averaged ERP and CSD waveforms at both hemispheres until 105 ms, as was the case in the study of Pang and Taylor (2002) as well. The ICA, nevertheless, revealed that the N1a activation of ERP-T80 and CSD-T84 clusters was present in response to standard-/atta/ already around the same latency of 80/84 ms as in response to EQ-/atta/. However, the CSD-T84 activated in a lesser degree in response to standard-/atta/ by showing activation of only one component with bilateral temporal sinks. In addition, another CSD-ICA component with bilateral temporal sinks activated in the N1a time window in response to standard-/atta/, while in response to EQ-/atta/ that component activated with reversed scalp distribution during Ta time window. This could indicate that the N1a activation in the short ISI condition is more bilateral and not as clearly dominated by left hemisphere activity as in the long ISI condition. This would be in line with the results obtained in the study of Pang and Taylor (2002).

Temporal positivity, Ta. In response to EQ-/atta/, a positivity at both temporal areas was seen during N1b time window in ERP and CSD topographies at 105 - 135 ms. As expected, the positivity was dominant at the right hemisphere, which was in line with the results reported by Bruneau and Gomot (1998). Radial temporal positivity was reflected in ICA clusters ERP-T112 and CSD-T107. The scalp distributions of CSD-T107 components were more localised than broad positivities in ERP-Ta components. The right hemisphere Ta was clearly more represented in ERP-T112 component than the left hemisphere Ta, while in CSD-T107 both hemisphere Ta-components were equally represented. Two of the ERP-T112 components with right temporal positivity, activated also in response to standard-/atta/, whereas the CSD-T107 did not activate as clearly in short ISI condition. Interestingly, CSD-T107 in response to EQ-/atta/ activated also at N2 time window, possibly suggesting that N2 elicited with long ISI might have an additional positive radial temporal component.

Temporal negativity, N1c. Negativities at temporoparietal areas were seen in grand averaged ERP and CSD waveforms only in response to EQ-/atta/ around 165 ms. They were more clearly observable from CSD waveforms. These negativities, thought to represent N1c activation, occurred here at about the same time range as in the studies of Bruneau and Gomot (1998) and Pang and Taylor (2002), where the N1c in children was seen at 170 ms. The late negative temporal activation was represented in ICA clusters ERP-T163 and CSD-T160. Components in ERP-T163 activated only at either right or left hemisphere, while cluster CSD-T160 included components with bilateral sinks too. In response to standard-/atta/, on the other hand, the N1c was not observable from grand averaged ERP nor CSD waveforms at all. Yet, the studies of Pang and Taylor (2000), Ponton et al. (2002) and Tonnquist-Uhlen et al. (2003) imply that the N1c can be elicited in children even with short ISIs as well. Inspection of selected N1c-ICA components revealed that only one CSD-ICA component from CSD-T160 cluster activated also in response to standard-/atta/. Thus the N1c activity in the short ISI condition was not very clearly present in this study.

Some of the radial temporal N1c ERP-ICA and CSD-ICA components showed inverted positive temporal activation earlier in latency reflecting Ta activation, and some N1c CSD-ICA components activated also during the N1a time window. This suggests that same brain generators are active at these different time windows. However, several of the temporal radial ICA components activated only at the time window of N1a, Ta or N1c. This indicates that the T-complex might not be as unitary complex as previously suggested in the literature, but

rather composed of separate sub-components that have at least partly independent activation patterns.

In addition to these abovementioned radial temporal clusters, temporal activation was seen in other ERP-ICA and CSD-ICA components as well, but their topographies indicated that they were produced by tangential source rather than radial. This corroborates the results of Tonnquist-Uhlen et al. (2003) and Ponton et al. (2002) of the existence of both radial T-complex and the temporal inversion of P1, N1b and P2 components produced by tangential sources.

Reliability of the ICA solutions. As mentioned in the introduction, there are some important presupposition to be considered before applying ICA. According to Brown et al. (2001) and Jung et al. (2001), the assumptions underlying the use of ICA include that 1) signals must be linearly mixed, 2) sources must be spatially stationary and temporally independent, 3) sources must be non-Gaussian and 4) the number of sources must be equal to or less than the number of recorded mixtures. When ICA is applied to high-density data, the EEG signals measured from the scalp are invariably linearly mixed by volume conduction and the number of recorded mixtures is high. Furthermore, in line with the assumptions is that underlying EEG sources in the brain are commonly assumed to be spatially stationary. In this study, the temporal independence of the underlying sources was attempted to be maximized by varying the experimental stimuli and conditions, thus minimizing the temporal overlap of the resulting ERP components. Furthermore, before applying ICA, the data was filtered and artefactual epochs were rejected in order to exclude the possible non-Gaussian sources like line noise and sensor noise. Also the guideline by Onton et al. (2006), of the sufficient amount of time points needed for reliable ICA decomposition, was followed. Thus, in this study, the prerequisites for ICA were considered to be fulfilled on a satisfactory level, and the resulting ICA solutions can, in this respect, be regarded as reliable.

Methodological considerations. In this study, N1-ICA components were identified and clustered in groups of N1-ICA sub-components based on their activation in response to EQ-/atta/ presented in with equal probability and a long ISI. Surprisingly, when assessing the activation of the selected components in response to standard-/atta/ presented with a short ISI, quite many of the components that were expected to activate in a short ISI condition, did not, however, show any activity. According to Luck (2005a), if a single component varies in latency across conditions, it may be treated by ICA as multiple components. In the study of

Karhu et al. (1997), the latency of N1 in children was slightly shortened in response to faster stimulus presentation. Thus in theory, it could be possible that ICA might isolate N1 activation in different conditions into different components. However, in this study, no differences in N1 latency produced by different conditions were observed from grand averaged waveforms.

Some of the ERP-ICA and CSD-ICA components activating during the N1 time window in response to EQ-/atta/ activated only for N1 whereas others showed activity around P1, P2 and/or N2 time windows as well. This would suggest that while there are some activation patterns that seem to be associated only to N1, there are also topographical distributions that are involved during activation of other ERP components as well. The same was observed in ICA study of Čeponienė et al. (2005), where it was concluded that N1 shared several independent components with P1 and P2. The temporal sources producing N1b, P1, P2 and N2 are all tangential and at least N1b and P1 dipoles have the same orientation (Ponton et al., 2002). Thus, it could be that the spatial proximity of the source generators and the partial temporal overlap of their activation time courses might have been too challenging for ICA to fully differentiate the scalp distributions produced by these different sources.

According to Onton et al. (2006), ICA is prone to point out intersubject variability due to a unique folding of every brain and differences in orientation of functionally analogous sources within participants. ICA, thus, may decompose a single process into several similar components that are contributed by different subsets of participants. This was evident from both ERP-ICA and CSD-ICA solutions investigated in this study. Most of the ERP-ICA and CSD-ICA component clusters that were identified were composed of several similar components. Each of the components was contributed by only 4 - 12 participants and most of the clusters included several very similar components. This could suggest that the similar components in one cluster might have represented slightly different manifestations of the same underlying process contributed by different sub-groups of participants, and also that one participant may have contributed to more than one component in the cluster. In this study, however, it was not investigated which of the participants contributed to which components, because that was beyond the scope of this Master's thesis. In the future research, however, this hypothesis could be studied by exploring component contributions more profoundly and possibly different of sub-groups of participants having somewhat different activation patterns could be identified. In the identification of different activation patterns of different sub-groups of participants, further statistical analysis of the components would also be useful.

Comparing ERP-ICA and CSD-ICA. In this study, both ERP-ICA and CSD-ICA approaches produced interpretable ICA components that could be associated to activation of underlying brain structures related to N1 sub-components. As hypothesised, CSD-ICA approach produced more precise and sharply defined components than ERP-ICA approach. Topographies of the components extracted with CSD-ICA approach were more accurate and localized when compared to the broadly distributed topographies of ERP-ICA components. The CSD-ICA approach was also assumed to lead to a decomposition of temporally more distinct and "peakier" activation patterns than the ERP-ICA approach. No differences, nevertheless, were observed in general shape of the activation time courses of CSD-ICA components when compared to ERP-ICA components.

CSD is known to emphasise local cortical activity over widespread volume conducted activity thus producing more focused topographies (Srinivasan, 2005). CSD is suggested to provide a more directly proportional estimate of the underlying generators of the electrical fields. While it is possible in the ERP, that a midline central maxima can be produced by either one source perpendicular to it or by bilateral sources, CSD will overcome this ambiguity by filtering out volume conducted activity propagating from distant areas (Bender et al., 2006). However, the non-specific N1 vertex component, that is suggested to be generated by a deep source (Hari et al., 1982), was extracted with ERP-ICA, but not identified at all among the CSD-ICA components. CSD is known to emphasises EEG signal that are generated by superficial sources projecting to relatively small areas of cortex, while activity of sources deep in the brain or produced by broad dipole layers may not be captured (Srinivasan, 2005).

The CSD-ICA approach seemed to compress the data into fewer ICA components activating in N1 time window than the ERP-ICA approach. Furthermore, several CSD-ICA components topographies included sources and sinks at two or more areas of the brain, suggesting that the activations of these different sources co-varied. As this might be true, it could also be, that the CSD-ICA was not able to properly separate the activation of these different structures. For instance, parietal activation was not isolated in separate CSD-ICA components, but merged into same components together with some other concurrent activities elsewhere in the brain. ICA returns as many ICA output components than there are recoding sensors used in the collection of the data. Thus, the decomposition of ERP waveforms produced 128 ERP-ICA components, whereas the decomposition of CSD waveforms returned only 81 CSD-ICA components. The CSD-ICA approach had to compress the data into less than 2/3 of the components that were available in ERP-ICA approach. In order to minimize this effect, it

would be worthwhile to preprocess the ERP data with PCA, in order to reduce the dimensionality of the ERP data into the same level as in the CSD data. In the future research, it would be informative to examine whether the ERP-ICA solution produced in this way, yielding to 81 PCA-preprocessed ERP-ICA components, would differ from the solution obtained with the approach applied in this study. This, however, was not possible to carry out in the scope of this Master's thesis.

Conclusions. From the results obtained here, it can be inferred that ICA was able to isolate N1 sub-components in response to EQ-/atta/ presented with equal probability and long ISI. The results of this study indicate that there are advantages and disadvantages in both ERP-ICA and CSD-ICA approach in analysing high-density averaged EEG data. CSD waveforms are useful in sharpening and summarising the broad ERP voltage topographies by producing more defined and focal components. However, activity of deep sources or widespread dipole layers might be better captured by ERP. Thus, it is informative to contrast both ERP and CSD data in clarifying the nature of ERP generators.

REFERENCES

Alcaini, M., Giard, M. H., Thévenet, M., & Pernier, J. (1994). Two separate frontal components in the N1 wave of the human auditory evoked response. *Psychophysiology*, 31, 611-615.

Amari, S. (1998). Natural gradient works efficiently in learning. *Neural Computation*,10, 251–276.

Bell, A. J., & Sejnowski, T. J. (1995). An information-maximization approach to blind separation and blind deconvolution. *Neural Computation, 7, 1129-1159.*

Bender, S., Oelkers-Ax, R., Resch, F., & Weisbrod, M. (2006). Frontal lobe involvement in the processing of meaningful auditory stimuli develops during childhood and adolescence. *NeuroImage*, 33, 759-773.

Brown, G. D., Yamada, S., & Sejnowski, T. J. (2001). Independent component analysis at the neural coctail party. *TRENDS in Neuroscience*, 24(1), 54-63.

Bruneau, N., & Gomot, M. (1998). Auditory evoked potentials (N1 wave) as indices of cortical development. In: Garreau, B., (Ed). *Neuroimaging in child neuropsychiatric disorders* (pp. 113-124). Berlin: Springer.

Cardoso, J.-F., & Laheld, B. (1996). Equivariant adaptive source separation. *IEEE Trans. on S.P., 45*(2), 434–444.

Čeponienė, R., Rinne, T., & Näätänen, R. (2002). Maturation of cortical sound processing as indexed by event-related potentials. *Clinical Neurophysiology*, 113, 870-882.

Čeponienė, R., Alku, P., Westerfield, M., Torki, M., & Townsend, J. (2005). ERPs differentiate syllable and non-phonetic sound processing in children and adults. *Psychophysiology*, 42, 391-406.

Cheour, M., Leppänen, P. H. T., & Kraus, N. (2000). Mismatch negativity (MMN) as a tool for investigating auditory discrimination and sensory memory in infants and children. *Clinical Neurophysiology*, 111, 4-16.

Coles, M. G. H., Gratton, G., & Fabiani, M. (1990). Event-related brain potentials. In J.T.Cacioppo & L. G. Tassinary (Eds.), *Principles of psychophysiology: Physical, social, and inferential elements* (pp. 413-455). Cambridge: Cambridge University Press.

Daruna, J. H., & Rau, A. E. (1987). Development of the late components of auditory brain potentials from early childhood to adulthood. In Johnson, R., Rohrbaugh, J.W., Parasuraman, R. (Eds.), *Current trends in event-related potential researc* (pp. 559-590). New York: Elsevier.

Delorme, A., & Makeig, S. (2004). EEGLAB: an open source toolbox for analysis of single-trial EEG dynamics including independent component analysis. *Journal of Neuroscience Methods*, 134, 9-21.

Dien, J., & Frishkoff, G. A. (2005). Principal components analysis of event-related potential datasets. In Handy, T. C. (Ed.), *Event-related potentials: a methods handbook*, (pp. 189-209). Cambridge, MA, UK: The MIT Press.

Donchin, E., & Heffley, E. (1978). Multivatiate analysis of event-related potential data: A tutorial review. In D. Otto (Ed.), *Multidisciplinary perspectives in event-related potential research*, (pp. 555-572). Washington, DC: U.S. Goverment Printing Office.

Eggermont, J. J., & Ponton, C. W. (2002). The neurophysiology of auditory perception: from single units to evoked potentials. *Audiology & Neuro-Otology*, 7, 71-99.

Giard, M. H., Perrin, F., Echallier, J. F., Thévenet, M., Froment, J. C., & Pernier, J. (1994). Dissociation of temporal and frontal components in the human auditory N1 wave: a scalp current density and dipole model analysis. *Electroencephalography and Clinical Neurophysiology*, 92, 238-252.

Goodin, D. S., Squires, K. C., Henderson, B. H., & Starr, A. (1978). Age-related variations in evoked potentials to auditory stimuli in normal human subjects. *Electroencephalography and Clinical Neurophysiology*, 44, 447-458.

Hari, R., Kaila, K., Katila, T., Tuomisto, T., & Varpula, T. (1982). Interstimulus interval dependence of the auditory vertex response and its magnetic counterpart: Implications for their neural generation. *Electroencephalography and Clinical Neurophysiology*, 54, 561-569.

Hyvärinen, A., & Oja, E. (2000). Independent component analysis: Algorithms and applications. Neural Networks, 13, 411-430.

Hämäläinen, J. A., Leppänen, P. H. T., Guttorm, T. K., & Lyytinen, H. (2007) N1 and P2 components of auditory event-related potentials in children with and without reading disabilities. *Clinical Neurophysiology* 118, 2263-2275.

Hämäläinen, J. A., Leppänen, P. H. T., Guttorm, T. K., & Lyytinen, H. (2008). Event-related potentials to pitch and rise time change in children with reading disabilities and typically reading children. *Clinical Neurophysiology*, 119(1), 100-115

Ille, N., Berg, P., Scherg, M. (2002). Artifact correction of the ongoing EEG using spatial filters based on artifact and brain signal topographies. *Clinical Neurophysiology*, 19, 113-124.

Johnson, M. H., de Haan, M., Oliver, A., Smith, W., Hatzakis, H., Tucker, L. A., & Csibra, G. (2001). Recoding and analyzing high-density event-related potentials with infants using the Geodesic sensor net. *Developmental Neuropsychology*, 19(3), 295-323.

Johnstone, S. J., Barry, R. J., Anderson, J. W., & Coyle, S. F. (1996). Age-related changes in child and adolescence event-related component morphology, amplitude and latency to standard and target stimuli in an auditory oddball task. *International Journal of Psychophysiology*, 24, 223-238.

Jung, T. P., Humphries, C., Lee, T.-W., Makeig, S., McKeown, M. J., Iragui, V., & Sejnowski T. (1998). Extended ICA removes artefacts from electroencephalographic recordings. *Advances in Neural Information Processing Systems*, 10, 229-235.

Jung, T.-P., Makeig, S., McKeown, M. J., Bell, A. J., Lee, T.-W., & Sejnowski. T. J. (2001). Imaging brain dynamics using independent component analysis. *Proceedings of the IEEE, Vol. 89, No. 7.*

Karhu, J., Herrgård, E., Pääkkönen, A., Luoma, L., Airaksinen, E., & Partanen, J. (1997). Dual cerebral processing of elementary auditory input in children. *NeuroReport*, 8, 1327-1330.

Kayser, J., & Tenke, C. E. (2006). Principal component analysis of Laplacian waveforms as a generic method for identifying ERP generator patterns: I. Evaluation with auditory oddball tasks. *Clinical Neurophysiology*, 117, 348-368.

Law, S. K., Rohrbaugh, J. W., Adams, C. M., & Eckardt, M. J. (1993). Improving spatial and temporal resolution in evoked EEG responses using surface Laplacians. *Electroencephalography and Clinical Neurophysiology*, 88, 309-322.

Lee, T. W., Girolami, M., & Sejnowski, T. J. (1999). Independent component analysis using an extended infomax algorithm for mixed subgaussian and supergaussian sources. *Neural Computation*, 11, 417-441.

Lee, T.-W., Girolami, M., Bell, A. J., & Sejnowski, T. J. (2000) A unifying information-theoretic framework for independent component analysis. *Computers & Mathematics with Applications*, 39(11), 1-21.

Leinonen, S., Müller, K., Leppänen, P.H.T., Aro, M., Ahonen, T., & Lyytinen, H. (2001). Heterogeneity in adult dyslexic readers: Relating processing skills to the speed and accuracy of oral text reading. *Reading and Writing*, 14(3-4), 265-296.

Leppänen, P.H.T., Richardson, U., Pihko, E., Eklund, K.M., Guttorm, T.K., Aro, M., & Lyytinen, H. (2002). Brain responses to changes in speech sound durations differ between infants with and without familial risk for dyslexia. *Developmental Neuropsychology*, 22, 407-422.

Liégeois-Chauvel, C., Musolino, A., Badier, J. M., Marquis, P., Chauvel P. (1994). Evoked potentials recorded from the auditory cortex in man: evaluation and topography of the middle latency components. *Electroencephalography and Clinical Neurophysiology*, 92(3,) 204-214.

Luck, S. J. (2005a). An introduction to the event-related potential technique. Cambridge, MA, UK: The MIT Press.

Luck, S. J. (2005b). Ten simple rules for designing ERP experiments. In Handy, T. C. (Ed.), *Event-related potentials: a methods handbook*, (pp. 17-32). Cambridge, MA, UK: The MIT Press.

Lutkenhöner, B., & Steinsträter O. (1998). High-precision neuromagnetic study of the functional organization of the human auditory cortex. *Audiol Neurootol*, 3, 191-213.

Lyytinen, H., Ahonen, T., Eklund, K., Guttorm T.K., Kulju, P., Laakso, M.-L., Leiwo, M., Leppänen, P.H.T., Lyytinen, P., Poikkeus, A.-M., Richardson, U., Torppa, M., & Viholainen, H. (2004). Early development of children at familial risk for dyslexia - Follow-up from birth to school age. *Dyslexia*, 10, 146-178.

Makeig, S., Jung, T.-P., Bell, A., Ghahremani, D., & Sejnowski, T. (1997). Blind separation of auditory event-related brain responses into independent components. *Neurobioloby, Vol. 94, 10979-10984.*

Makeig, S., Westerfield, M., Jung, T.-P., Covington, J., Townsend, J., Sejnowski, T. J., & Courchesne, E., (1999). Functionally independent components of the late positive event-related potential during visual spatial attention. *The Journal of Neuroscience 19(7), 2665-2680.*

McCallum, W.C., & Curry, S.H. (1980). The form and distribution of auditory evoked potentials and CNVs when stimuli and responses are latealized. In H.H. Kornhuber, L. Decke (Eds.), *Progress in brain research* (pp. 117-163). Amsterdam: Elsevier.

Nunez P.L., & Srinivasan, R. (2006). *Electric Fields of the Brain: The neurophysics of EEG* (2nd ed.), Oxford University Press, New York.

Nunez, P. (1981). Electric fields of the brain. New York: Oxford University Press.

Näätänen, R. (1990). The role of attention in auditory information processing as revealed by event-related potentials and other brain measures of cognitive function. *Behavioral and Brain Sciences*, 13(2), 201-288.

Näätänen, R., & Picton, T. (1987). The N1 wave of the human electric and magnetic response to sound: a review and an analysis of the component structure. *Psychophysiology*, 24, 375-425.

Onton, J., Westerfield, M., Townsend, J., & Makeig, S. (2006). Imaging human EEG dynamics using independent component analysis. *Neuroscience and Biobehavioral Reviews, 30, 808-822.*

Pang, E. W., & Taylor, M. J. (2000). Tracking the development of the N1 from age 3 to adulthood: an examination of speech and non-speech stimuli. *Clinical Neurophysiology* 111, 388-397.

Perrin, F., Pernier, J., Bertrand, O., & Echallier, J.F. (1989). Spherical splines for scalp potential and current density mapping. *Electroencephalography and Clinical Neurophysiology*, 72, 184-187.

Picton, T. W., Hillyard, S. A., Krausz, H. I., & Galambos, R. (1974). Human auditory evoked potentials: I. Evaluation of components. *Electroencephalography and Clinical Neurophysiology*, 36, 179-190.

Ponton, C. W., Eggermont, J. J., Kwong, B., & Don, M. (2000). Maturation of human central auditory system activity: evidence from multi-channel evoked potentials. *Clinical Neurophysiology*, 111, 220-236.

Ponton, C. W., Eggermont, J. J., Khosla, D., Kwong, B., & Don, M. (2002). Maturation of human central auditory system activity: separating evoked potentials by dipole source modeling, *Clinical Neurophysiology*, 113, 407-420.

Regan, D. (1989). *Human brain electrophysiology: Evoked potentials and evoked magnetic fields in science and medicine.* New York: Elsevier.

Scherg, M., & von Cramon, D. (1985). Two bilateral sources of the late AEP as identified by a spatio-temporal dipole model. *Electroencephalography and Clinical Neurophysiology*, 62, 32-44.

Sharma, A., Kraus, N., McGee, T.J., & Nicol, T.G. (1997). Developmental changes in P1 and N1 central auditory responses elicited by consonant-vowel syllables. *Electroencephalography and Clinical Neurophysiology*, 104, 540-545.

Srinivasan, R. (2005). Hihg-resolution EEG: Theory and practice. In T.C. Handy (Ed.), *Event-related potentials*, (pp. 167-188). Cambridge, MA, US: The MIT Press.

Stone, J. (2002). Independent component analysis: an introduction. *TRENDS in Cognitive Sciences,* 6 (2).

Tonnquist-Uhlen, I., Ponton, C. W., Eggermont, J. J., Kwong, B., & Don, M. (2003). Maturation of human central auditory system activity: T-complex. *Clinical Neurophysiology*, 114, 685-701.

Vaughan, H. G., Jr., & Ritter W. (1970). The sources of auditory evoked responses recorded from the human scalp. *Electroencephalography and Clinical Neurophysiology*, 28, 360-367.

Wolpaw, J. R., & Penry J. K. (1975). A temporal component of the auditory evoked response. *Electroencephalography and Clinical Neurophysiology*, 39, 609-620.